

Tectonics

RESEARCH ARTICLE

10.1029/2017TC004687

Key Points:

- New seismic lines document the geological evolution of key structures at the Aden-Owen-Carlsberg triple junction
- The Beautemps-Beaupré Basin opened at 2.4 Ma, coeval with the formation of the 800-km-long Owen Fracture Zone
- The 2.4-Myr-old reorganization of the India-Arabia Plate boundary is unrelated to any known kinematic change

Correspondence to:

M. Rodriguez,
rodriguez@geologie.ens.fr

Citation:

Rodriguez, M., Fournier, M., Chamot-Rooke, N., Huchon, P., & Delescluse, M. (2018). The geological evolution of the Aden-Owen-Carlsberg triple junction (NW Indian Ocean) since the late Miocene. *Tectonics*, 37, 1552–1575. <https://doi.org/10.1029/2017TC004687>

Received 2 JUN 2017

Accepted 14 FEB 2018

Accepted article online 25 APR 2018

Published online 27 MAY 2018

The Geological Evolution of the Aden-Owen-Carlsberg Triple Junction (NW Indian Ocean) Since the Late Miocene

Mathieu Rodriguez¹ , Marc Fournier² , Nicolas Chamot-Rooke¹ , Philippe Huchon², and Matthias Delescluse¹ 

¹Laboratoire de Géologie, Ecole normale supérieure, CNRS, PSL Research University, Paris, France, ²Sorbonne Universités, UPMC Université Paris 06, Paris, France

Abstract The Aden-Owen-Carlsberg triple junction is the place where Arabia, Somalia, and India meet in the Arabian Sea (NW Indian Ocean). Here we present a new seismic data set crossing a key structure of the triple junction, namely, the Beautemps-Beaupré pull-apart basin at the southern end of the Owen Fracture Zone. The seismic data set is tied to Ocean Drilling Program Leg 117 Sites at the top of the Owen Ridge, which provides a detailed tectono-stratigraphic framework since the Late Miocene. We show that the triple junction configuration has been disturbed by a major kinematic change at ~8 Ma and since then experienced a series of transient structural adjustments. A major structural episode is recorded at 2.4 Ma, expressed by the opening of the Beautemps-Beaupré Basin and the uplift of its southern flank (the Beautemps-Beaupré Ridge). This episode is coeval with the formation of the present-day Owen Fracture Zone and must be considered as a part of a major structural reorganization of the entire India-Arabia plate boundary up to the Makran subduction zone. This 2.4-Myr-old geological episode is unrelated to any significant kinematic change, leaving questions over its driving mechanism.

1. Introduction

In plate tectonics, triple junctions are defined as places where three plates and their boundaries meet (Cronin, 1992; McKenzie & Morgan, 1969). The Aden-Owen-Carlsberg (AOC) triple junction in the NW Indian Ocean is located at the contact between Arabia, Somalia, and India (Figure 1). The AOC triple junction was initially described as a Ridge-Fault-Fault triple junction (Gordon & DeMets, 1989; McKenzie et al., 1970; Wilson, 1965), which involves the Sheba Ridge, the Owen Transform connecting the Carlsberg Ridge, and the Owen Fracture Zone (OFZ) connecting the Makran subduction zone. In detail, the present-day configuration of the AOC triple junction is more complex (Fournier, Chamot-Rooke, et al., 2008; Fournier, Petit, et al., 2008; Fournier et al., 2001). Strike-slip motion along the OFZ turns into diffuse extension instead of directly connecting the Sheba spreading center (Figure 1). The area of active extension is expressed by a conspicuous pull-apart basin, referred to as the Beautemps-Beaupré Basin (abbreviated below as B3; Figures 1 and 2), which is located ~280-km north of the Sheba Ridge's axis. The present-day configuration of the AOC triple junction corresponds to a transient stage from an unstable Ridge-Fault-Fault configuration to a future more stable configuration (Fournier et al., 2001; Fournier, Chamot-Rooke, et al., 2008; Fournier, Petit, et al., 2008). The present-day configuration of the AOC triple junction is therefore similar to the Açores (Miranda et al., 2010) and the Juan Fernandez (Bird et al., 1998) triple junctions (in the Atlantic and Pacific Oceans, respectively).

A seismic data set acquired during the OWEN-2 cruise in 2012 revealed that the uplift of the Owen Ridge, a series of bathymetric highs identified along the OFZ, began at 8.2–8.8 Ma (Rodriguez, Chamot-Rooke, Huchon, Fournier, & Delescluse, 2014), and that major pull-apart basins of the OFZ started opening at 2.4 Ma (Rodriguez et al., 2013; Rodriguez, Chamot-Rooke, Huchon, Fournier, Lallemand, et al., 2014). Although these geological events suggest a complex evolution of the AOC triple junction since the Late Miocene, the precise timing of its changes of configuration remains unconstrained (Fournier et al., 2010).

Here we present a new set of multibeam data, echosounder, and seismic profiles crossing key structures formed at the AOC triple junction (mainly the Beautemps-Beaupré Basin), which allows us to build a detailed structural evolution of the area. The objectives of this study are (1) to identify the successive geological events involved in the evolution of the triple junction from the Ridge-Fault-Fault configuration to the currently incipient Ridge-Ridge-Ridge configuration, (2) to constrain the relative chronology of these successive geological events from ties of the seismic data set with Ocean Drilling Program (ODP) Sites and spatial

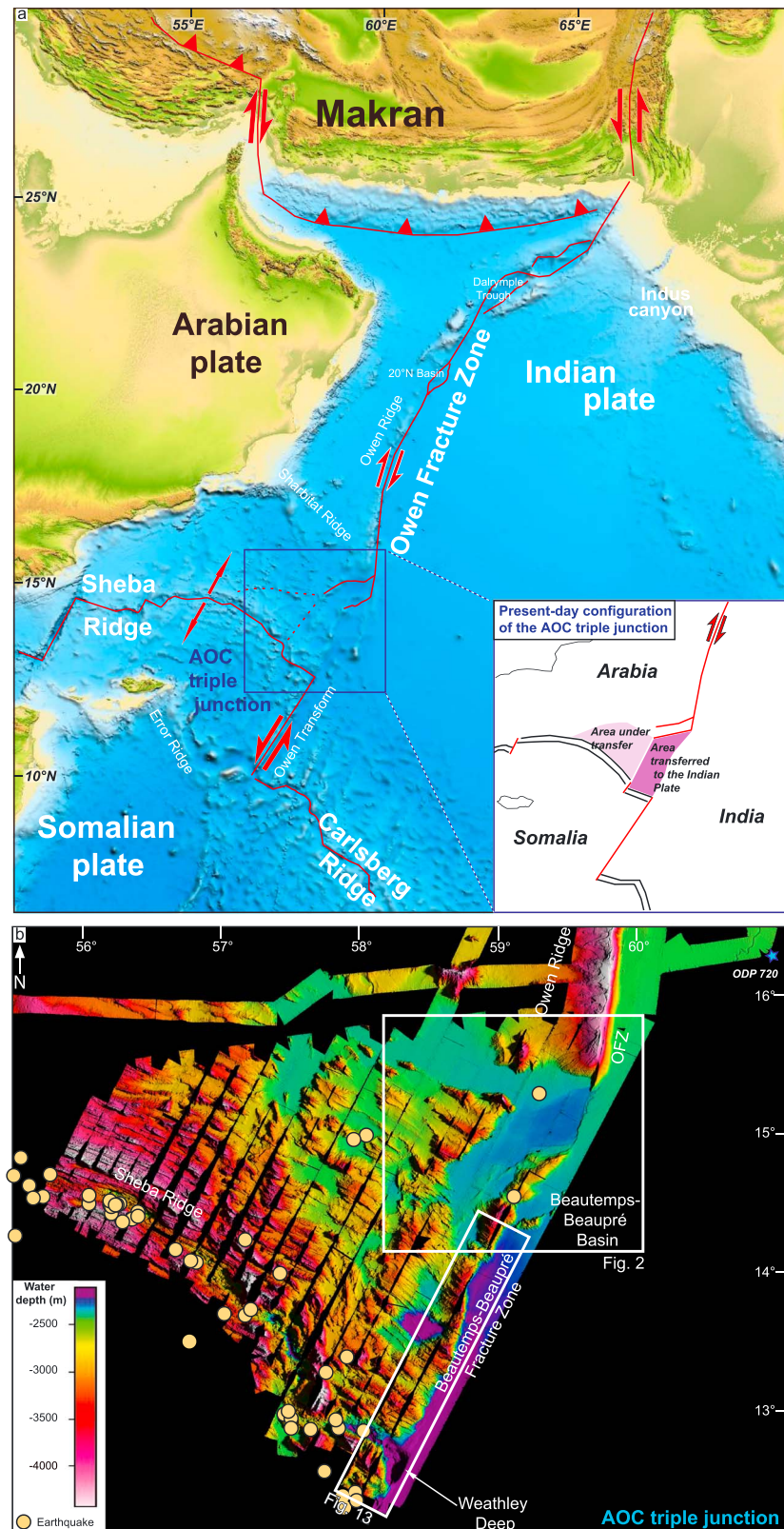


Figure 1. (a) Simplified tectonic map of the Arabian Sea. The inset represents simply the AOC triple junction structure (modified from Fournier, Petit, et al., 2008). (b) Multibeam bathymetry of the Aden-Owen-Carlsberg (AOC) triple junction. OFZ: Owen Fracture Zone. Seismicity from CMT Harvard catalog ($M_w > 4$).

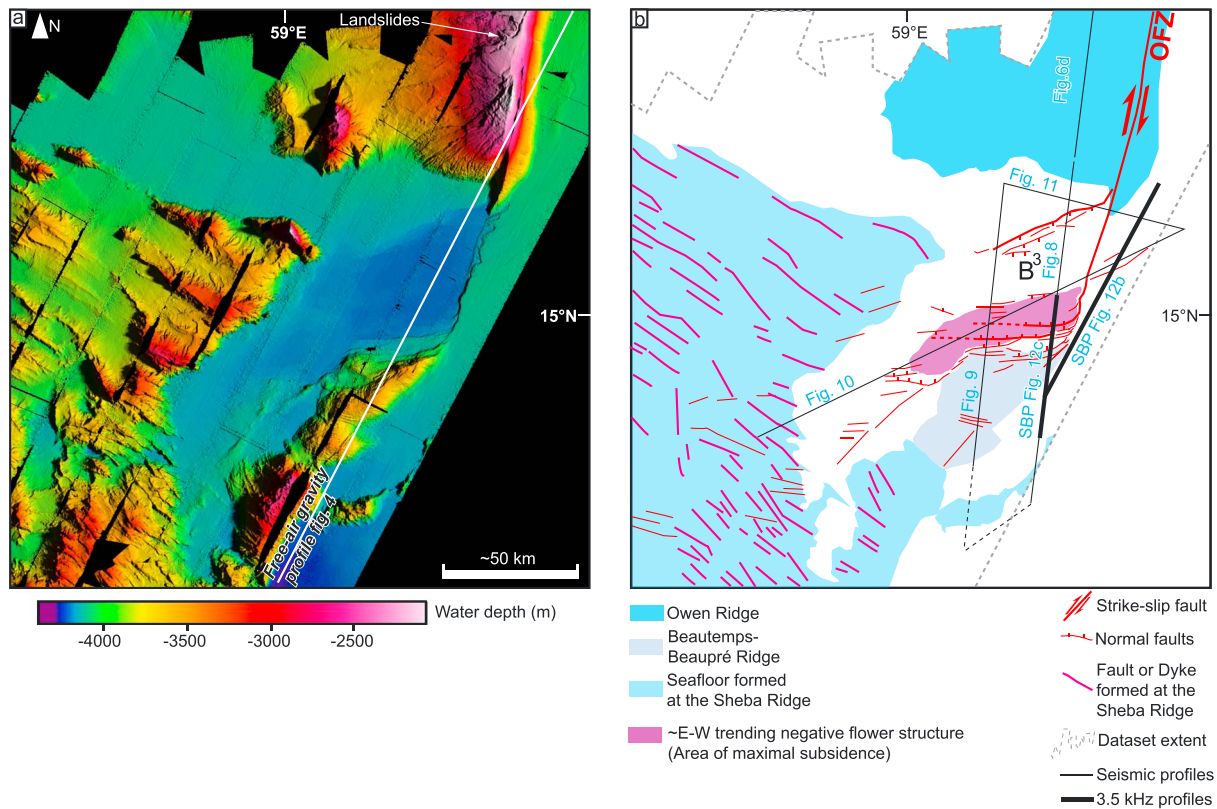


Figure 2. (a) Enlargement of the multibeam data of the Beautemps-Beaupré Basin and Ridge. (b) Structural sketchmap of the Beautemps-Beaupré Basin and Ridge system, with locations of the seismic lines investigated in this study.

correlation of regional-scale geological markers, and (3) to identify the potential drivers of the changes of configuration of the AOC triple junction since the Late Miocene.

2. Geological Background

2.1. Present-Day Configuration of the Aden-Owen-Carlsberg Triple Junction

The earthquake distribution in the vicinity of the AOC triple junction (Figure 1) suggests that deformation is currently occurring around the margins of a triangle-shaped microplate composed of oceanic lithosphere accreted north of the Sheba Ridge (Fournier et al., 2001; Fournier, Chamot-Rooke, et al., 2008; Fournier, Petit, et al., 2008). The microplate is being transferred from Arabia to India since the beginning of the ongoing reorganization of the triple junction (Figure 1; Fournier, Chamot-Rooke, et al., 2008; Fournier, Petit, et al., 2008). The actual triple junction lies at the Sheba Ridge, ~300 km west of the Wheatley Deep, where the Sheba Ridge joins the Owen Transform (Figure 1). According to the distribution of earthquake foci (Fournier et al., 2001; Fournier, Chamot-Rooke, et al., 2008; Fournier, Petit, et al., 2008), the OFZ and the Owen Transform (i.e., the ~250-km-long sinistral India-Somalia plate boundary) are currently disconnected.

A ~200-km-long series of oceanic ridges, including the Varun Bank, on top of which peridotites have been dredged (Exon, 2011), is better imaged on the free-air gravity anomaly map on the eastern side of the B3 (Figure 3a). Their trend is oblique to the trend of the Owen Transform by 15°. A vintage seismic line (Cochran, 1978) shows a fossil fault system buried under the Indus sediments on their eastern side (Figure 3b). The origin of this series of oceanic ridges remains unknown. They may be tentatively interpreted as transpressive ridges formed along the fracture zone, similar to oceanic transverse ridges observed along the Saint-Paul and Vema Transforms in the Atlantic Ocean (Bonatti et al., 2005; Maia et al., 2016).

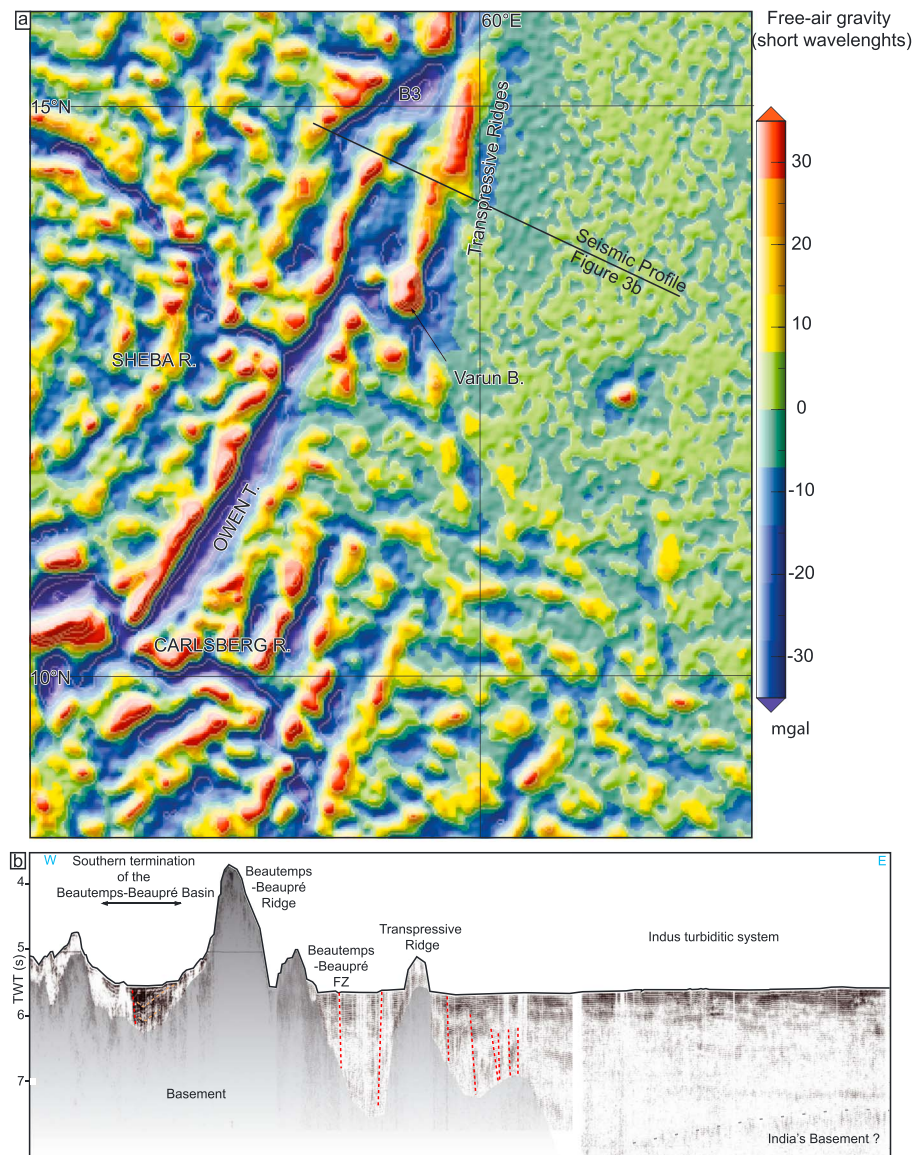


Figure 3. (a) Free-air gravity anomaly map of the Aden-Owen-Carlsberg triple junction, filtered for short wavelengths from DTU 13 database (Andersen et al., 2013). B3: Beautemps-Beaupré basin, R. = ridge, B. = bank, T. = transform). (b) Vintage seismic line; cruise VEMA V3502, <https://doi.org/10.7284/906184> (Cochran, 1978) crossing the Aden-Owen-Carlsberg triple junction and the distal Indus fan (see location on Figure 3a).

2.2. The Beautemps-Beaupré Basin

The B3 is the key structure at the AOC triple junction. It is a 120-km-long, 50-km-wide rhomboedric pull-apart basin (Figure 2; Fournier, Chamot-Rooke, et al., 2008; Fournier, Petit, et al., 2008). The B3 is bounded to the east by the southern termination of the OFZ (Figure 2). A diffuse system of N70–N90°E trending normal faults constitutes the northern and southern boundaries of the B3, while the western boundary of the basin is loosely defined on the multibeam map (Figure 2; Fournier, Chamot-Rooke, et al., 2008; Fournier, Petit, et al., 2008). A large, ~100 mGal free-air anomaly is recorded at the B3 (Figure 4; Fournier, Chamot-Rooke, et al., 2008). The subsidence of the basin over ~3 km may explain the gravity anomaly (Fournier, Chamot-Rooke, et al., 2008). The B3 only forms an ~100-m-deep depression with respect to the surrounding seafloor (Fournier, Chamot-Rooke, et al., 2008). The relatively subtle bathymetric expression of the B3 results from the competition between its subsidence and the high turbiditic sedimentation rates, ranging between 137

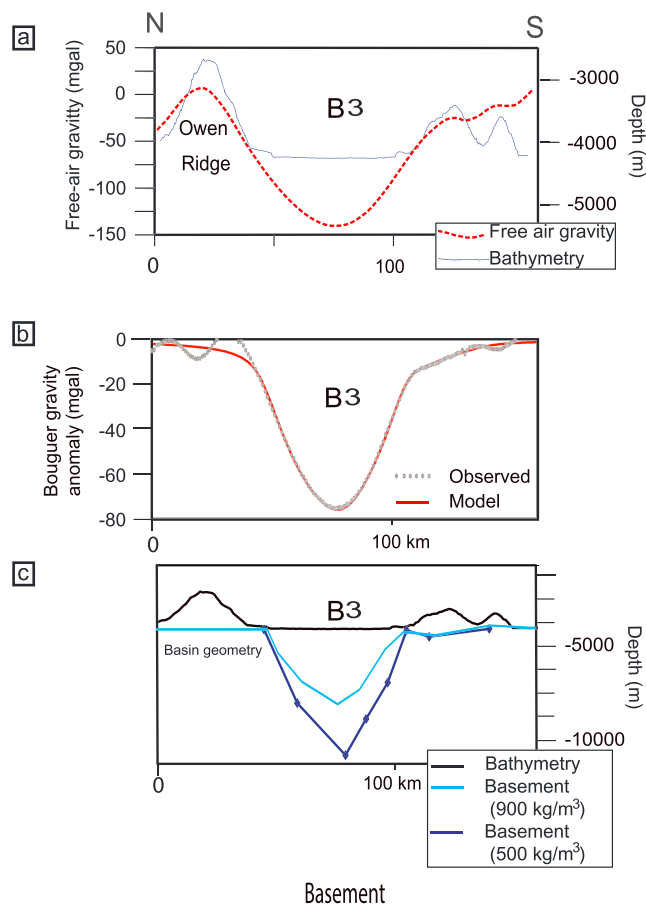


Figure 4. (a) Free-air gravity profile crossing the Beautemps-Beaupré Basin, from Fournier, Petit, et al. (2008); see Figure 2a for location. (b) Bouguer gravity anomaly profile, observed and calculated. (c) Basement geometries of the Beautemps-Beaupré Basin, derived using a density contrast between the basin fill and the basement of 500 and 900 kg/m³. B3: Beautemps-Beaupré Basin. Marine Bouguer anomaly was calculated by correcting two types of effects: (1) local positive reliefs along the profile on both sides of the B3, assumed to be mainly made of crustal shoulders (all reliefs above the mean depth of the B3, that is, 4,265 m, were corrected for assuming a 2,600 kg/m³ density or density contrast with water of 1,600 kg/m³); (2) a regional long-wavelength effect depressing the gravity field beyond the sole effect of the B3. The resulting marine Bouguer is interpreted as being due to a single basement interface, with a density contrast ranging from -500 kg/m³ (e.g., sediments versus oceanic crust) to -900 kg/m³ (e.g., sediments versus mantle). The basin is assumed to be uncompensated: Any compensation at depth would require a deeper basement.

unconformities) of their activity (Rodríguez, Chamot-Rooke, Huchon, Fournier, & Delescluse, 2014; Rodríguez, Chamot-Rooke, Huchon, Fournier, Lallemand, et al., 2014). Early Miocene to Late Miocene sediments preserved on the top of the southern segment of the Owen Ridge display a fanning configuration, and a dense fault system, which may reflect either remnants of strike-slip tectonics prior to the Owen Ridge uplift, or differential compaction processes, distinct from plate boundary tectonics (Rodríguez, Chamot-Rooke, Huchon, Fournier, & Delescluse, 2014; Rodríguez et al., 2016).

2.4. The Owen Ridge

The Owen-Murray Ridge consists of a series of bathymetric highs running along the OFZ (Matthews, 1966). The top of the basement of the Owen Ridge is composed of Paleogene trachybasalts (Shipboard Scientific Party, 1989). The Owen Ridge basement was covered by turbidites up until the time of 15 Ma (Figure 6).

and 944 m/Myr at the nearby ODP Site 720 (see Figure 1b for location) since 1.1 Ma (Shipboard Scientific Party, 1989). Except for the master faults bounding the basin, most of the normal faults remain blind on the seafloor (Figure 2).

2.3. The Owen Fracture Zone and the Successive Generations of the India-Arabia Plate Boundary

The OFZ is the 800-km-long dextral strike-slip India-Arabia plate boundary connecting the AOC triple junction to the Makran Subduction Zone (Fournier et al., 2011; Rodríguez et al., 2011). Morphological offsets of the Owen Ridge on the order of 10–12 km are consistent with an age of emplacement of the OFZ around 3–6 Ma, assuming that the current motion of 3 ± 1 mm/year continued steadily for this time span (DeMets et al., 2010; Fournier et al., 2011; Rodríguez et al., 2011). The OFZ displays remarkable pull-apart basins along its strike, including the 90-km-long, 35-km-wide 20°N Basin (Fournier et al., 2011; Rodríguez et al., 2011, 2013), and the 150-km-long, 30-km-wide Dalrymple Trough (between ~ 22 and 23° N), which forms an horsetail structure at the northern termination of the OFZ (Edwards et al., 2000; Fournier et al., 2011; Gaedicke et al., 2002; Rodríguez, Chamot-Rooke, Huchon, Fournier, Lallemand, et al., 2014). The reflector marking the opening of both the 20°N Basin and the Dalrymple Trough can be tracked from line to line, as far as the top of the southern Owen Ridge, where ODP Sites (721, 722, and 731) provide detailed stratigraphic constraints (Figure 5; Shipboard Scientific Party, 1989). There, this key reflector is dated at 2.4 Ma, in agreement with age estimates from geological markers in the vicinity of the main pull-apart basins (Rodríguez, Chamot-Rooke, Huchon, Fournier, Lallemand, et al., 2014). The reflector recording the opening of the pull-apart basins along the OFZ can be traced to the Oman abyssal plain, in front of the Makran accretionary wedge, where it merges with the M-unconformity (Ellouz Zimmermann et al., 2007; Rodríguez, Chamot-Rooke, Huchon, Fournier, Lallemand, et al., 2014). The regional-scale seismic correlation of the key, 2.4-Myr-old reflector marking the opening of pull-apart basins along the OFZ is provided in Figure 5.

The configuration of the India-Arabia plate boundary prior to the inception of the OFZ is still enigmatic. Preliminary kinematic reconstructions based on magnetic anomalies from the Sheba and Carlsberg Ridges suggest about 80 km of dextral relative motion since ~ 20 Ma (Chamot-Rooke et al., 2009). However, the significance of fracture zone offsets identified at the eastern edge of the Owen Ridge under the Indus turbidites remains ambiguous because of the lack of a clear sedimentary record (i.e., fanning configuration of the sediments and

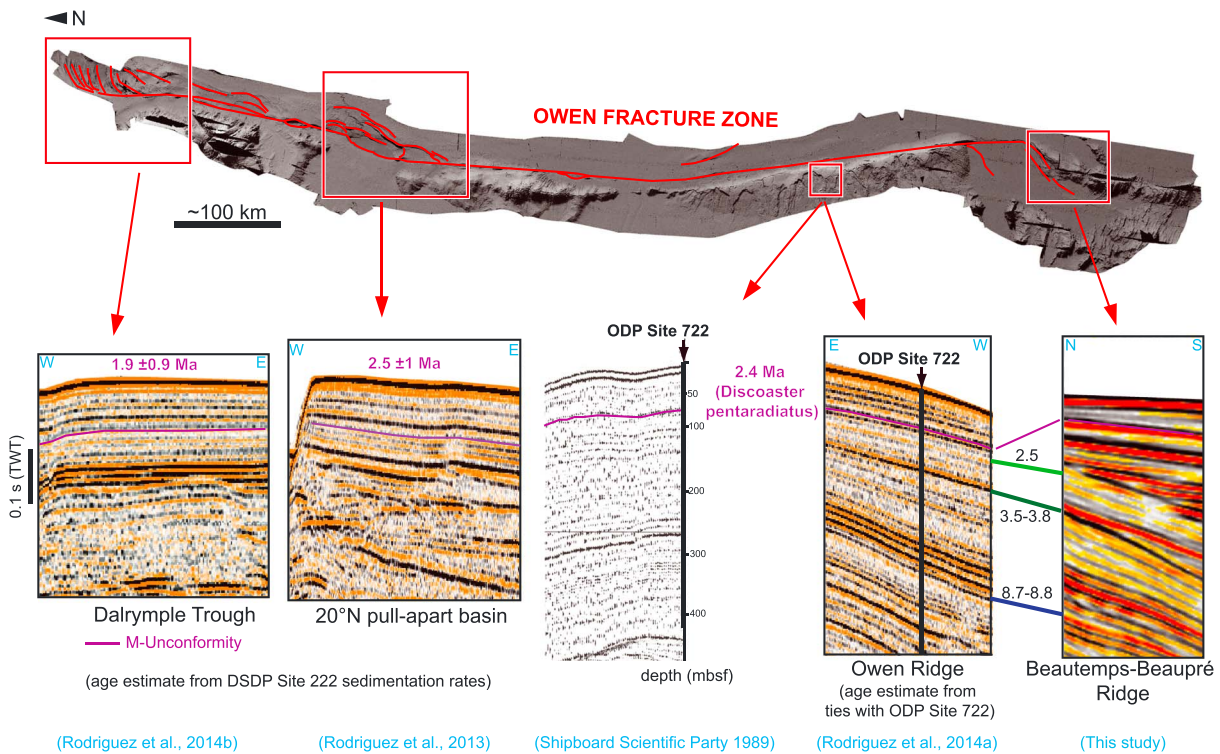


Figure 5. Regional correlation of the reflector marking the structural reorganization of the entire India-Arabia plate boundary at 2.4 Ma at the edges of the Dalrymple Trough and the 20°N Basin, at the top of the Owen Ridge, and at the Beautemps-Beaupré Ridge. This key reflector can be easily tracked from line to line within the pelagic cover that blankets the area since the late Pliocene, except at the Beautemps-Beaupré Basin and Ridge where turbidites are inter bedded within the pelagites.

Since then, the Owen Ridge has been only covered by pelagic sediments (Figure 6; Shipboard Scientific Party, 1989). The uplift of the Owen-Murray Ridge initiated between 8.2 and 8.8 Ma (Rodriguez, Chamot-Rooke, Huchon, Fournier, & Delescluse, 2014; Rodriguez, Chamot-Rooke, Huchon, Fournier, Lallemand, et al., 2014). The uplift is recorded by an angular unconformity along the edge of the Owen-Murray Ridge, a conspicuous fanning configuration of Indus sediments at the southern Owen Ridge, and numerous landslide deposits (Rodriguez et al., 2012; Rodriguez, Chamot-Rooke, Huchon, Fournier, and Delescluse, 2014; Rodriguez, Chamot-Rooke, Huchon, Fournier, Lallemand, et al., 2014). A coeval episode of deformation is observed along the southeastern Oman margin (Rodriguez, Chamot-Rooke, Huchon, Fournier, and Delescluse, 2014; Rodriguez et al., 2016).

The initiation of the uplift of the Owen-Murray Ridge is coincident in time with the kinematic change affecting the entire Indian Ocean around 8 Ma. This kinematic change is expressed by the onset of intraplate deformation in the Central Indian Ocean separating India from Australia (Bull et al., 2010; Bull & Scrutton, 1990, 1992; Chamot-Rooke et al., 1993; Delescluse & Chamot-Rooke, 2007; Delescluse et al., 2008; Henstock & Minshull, 2004; Krishna et al., 2009; Weissel et al., 1980, 1992; Wiens et al., 1985), and to the separation of Somalia from Nubia related to the East African Rift system (DeMets et al., 2005; DeMets & Merkouriev, 2016). The origin of this kinematic change is unclear. The most commonly invoked driver is a change of the gravitational potential energy gradient related to the growth of the Himalaya-Tibet (Molnar & Stock, 2009). Alternatively, Iaffaldano and DeMets (2016) proposed that this kinematic change could correspond to a global plate reorganization event driven by changes in the dynamics of the Pacific plate.

2.5. The Sheba Ridge

The Sheba Ridge is an oceanic spreading center initiated about 20 Ma (Chron 6A, 19.7 Ma) along the Owen Transform, which subsequently propagated westward into the Gulf of Aden toward the Afar Hotspot (d'Acremont et al., 2006, 2010; Fournier et al., 2010; Leroy et al., 2010). In its easternmost segment, the Sheba Ridge formed in the south of the Owen Basin (Figure 1). The nature and the age of the Owen basin

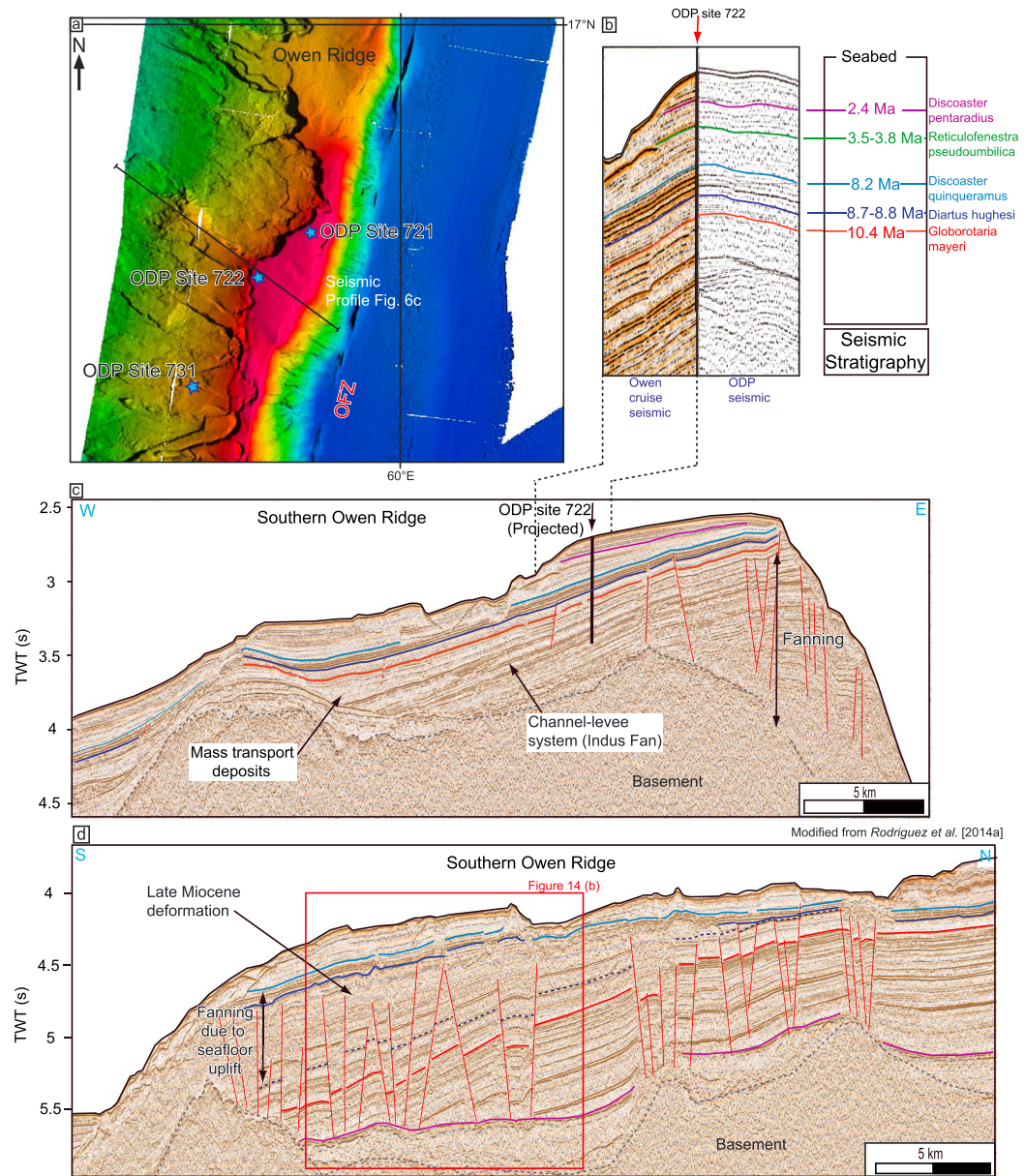


Figure 6. (a) Multibeam bathymetry of the segment of the southern Owen Ridge, where the ODP Sites used for the stratigraphic framework of this study are located. OFZ: Owen Fracture Zone. (b) Stratigraphy from ODP sites, and correlation between the ODP seismic data set and the OWEN 2 seismic data set. The colors correspond to key seismic horizons on the seismic profiles. (c) Ties of ODP Site 722 with the seismic data set crossing the Owen Ridge following a W-E direction. (d) Ties of ODP Sites with the seismic data set crossing the Owen Ridge following a S-N direction. For details of the ties, the reader is referred to Shipboard Scientific Party (1989) and Rodriguez, Chamot-Rooke, Huchon, Fournier, and Delescluse (2014).

are a matter of debate due to a lack of a magnetic data capable of revealing seafloor spreading anomalies less ambiguously (Gaina, van Hinsbergen, & Spakman, 2015; Mountain & Prell, 1990; Rodriguez et al., 2016). The identification of Paleogene trachybasalts at the available drilling sites in the eastern part of the Owen Basin (Shipboard Scientific Party, 1974, 1989) suggests an oceanic lithosphere. In this framework, the first stage of formation of the Sheba Ridge follows an intraoceanic episode of rifting and therefore constitutes a case of Ocean-Ocean Transition (Stein & Cochran, 1985).

The Sheba Ridge formed shortly after a global plate reorganization event recorded at 24 Ma (chron 6C), expressed by a reorganization of all the spreading centers of the Indian Ocean (Patriat et al., 2008). After

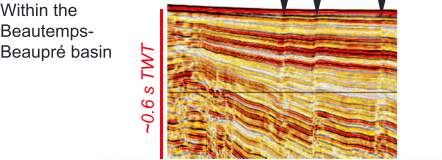
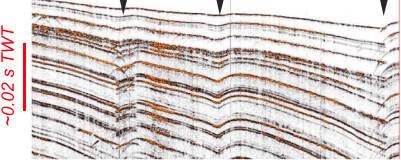
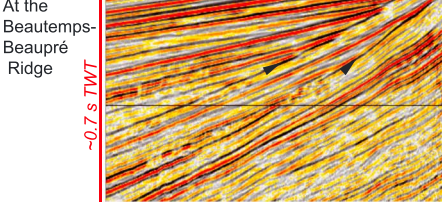
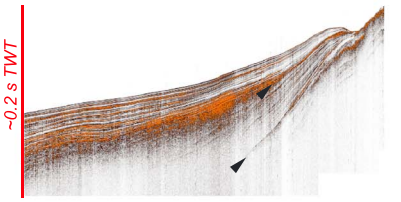
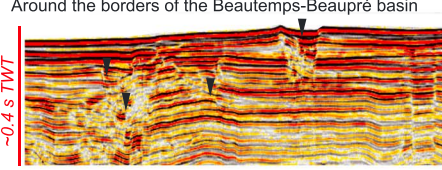
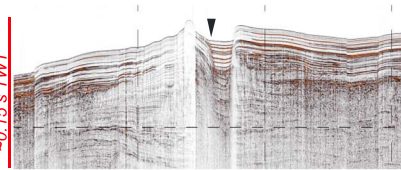
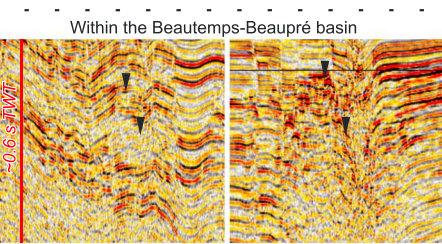
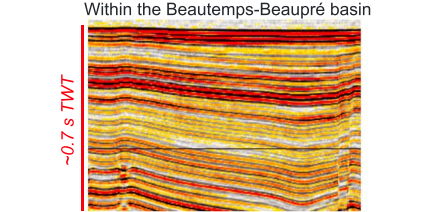
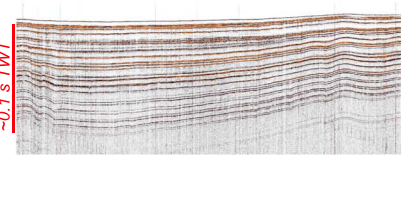
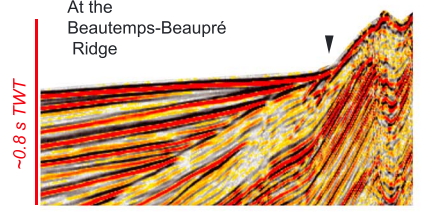
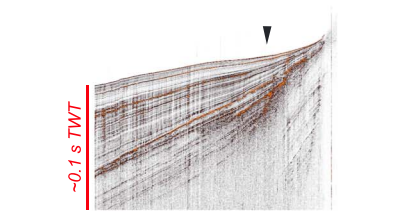
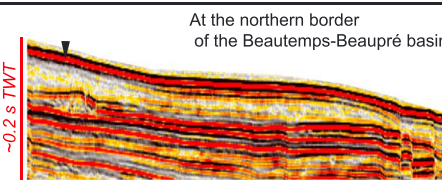

Sedimentary Feature	Seismic Facies	3.5 kHz Facies	Description/ Criteria of Identification
Fanning/ Growth fault	Within the Beautemps-Beaupré basin 		<ul style="list-style-type: none"> Fanning configuration of the deposits Increase of fault offset with depth
Angular unconformities	At the Beautemps-Beaupré Ridge 		<ul style="list-style-type: none"> Tilted pelagic unit progressively onlapped by turbidites
Turbiditic channel-levee systems from the Indus Fan	Around the borders of the Beautemps-Beaupré basin 		<ul style="list-style-type: none"> Channel axes: lens-like architecture with high-amplitude reflection Levees: wedge shape, high amplitude transparent facies Example of a system of faults, which offsets some channel-levee systems close to their axis
	Within the Beautemps-Beaupré basin 	No available 3.5 kHz profiles at this depth	
Ponded Turbidites	Within the Beautemps-Beaupré basin 		<ul style="list-style-type: none"> Transparent facies, strongly reflective base
Contourite deposits	At the Beautemps-Beaupré Ridge 		<ul style="list-style-type: none"> Aggradation of deposits non parallel to the accumulation surface Sigmoid configuration of the sedimentary body (lateral thickness variations and pinching of sedimentary layers)
Mass transport deposits	At the northern border of the Beautemps-Beaupré basin 		<ul style="list-style-type: none"> Hyperbolic to chaotic reflections, with a transparent seismic facies

Figure 7. Classification of the sedimentary features observed in the vicinity of the Aden-Owen-Carlsberg triple junction on seismic and subbottom profiles, and their criteria of identification. The black arrows point areas where the features can be well observed.

this episode, spreading rates gradually decreased until the plate reorganization event at ~8 Ma. Since then, seafloor spreading rates have remained steady (DeMets et al., 2005; DeMets & Merkouriev, 2016; DeMets et al., 2015; Fournier et al., 2010; Merkouriev & DeMets, 2006).

3. Data Set and Methods

3.1. Data Set

The data set presented in this study was acquired onboard the BHO Beautemps-Beaupré (a ship of the French Naval Hydrographic and Oceanographic Service) during the AOC, OWEN- FANINDIEN, and OWEN-2 surveys in 2006, 2009, and 2012, respectively. The multibeam bathymetry was collected using a Kongsberg-Simrad EM 120 echosounder, producing a DEM at 80 m grid interval. The SBP120 subbottom profiler provided a coincident set of high-frequency (3.5 kHz), high-resolution profiles with penetration down to 100 m in fine grained sediments. Seismic reflection profiles were acquired using the high-speed (10 knots) seismic device designed by GENAVIR. The source consists of two GI air guns (one 105/105 c.i. and one 45/45 c.i.) fired every 10 s at 160 bars in harmonic mode, resulting in frequencies ranging from 15 to 120 Hz. The receiver is a 24-channel, 300-m-long seismic streamer, allowing a common midpoint spacing of 6.25 m and a subsurface penetration of about 2 s two-way travel time (TWT). The processing consisted of geometry setting, water-velocity normal moveout, stacking, water-velocity Kirchhoff poststack time migration, band-pass filtering, and automatic gain control. All profiles are displayed with a vertical exaggeration of ~13 at the seafloor.

3.2. Seismic Interpretation of the Sedimentary Features

The identification of sedimentary features and key configurations commonly observed on the seismic and 3.5 kHz data set are based on the following criteria (summarized in Figure 7). The distal Indus turbiditic fan in the opened abyssal plain displays typical channel-levee systems (Clift et al., 2001). The axis of a channel is characterized by a typical lens-like architecture and a concave-up lower boundary, with a discontinuous, high-amplitude reflection at the base. The associated turbiditic levees have a wedge shape, with a high-amplitude, transparent seismic facies (Figure 7). In contrast with the Indus abyssal plain, the B3 constitutes a confined area of deposition, which results in a different turbidite facies (Bourget et al., 2013); hereafter referred as ponded turbidites. This seismic facies results from turbidity currents becoming trapped in the basin and repeatedly reflected from its walls (McHugh et al., 2006). The resulting oscillations of the turbidite plume lead to strong sediment sorting, with coarse grains at the bottom of the sequence forming the high-amplitude reflectors and fined grained coming from the muddy part of the turbiditic flow at the origin of the transparent facies (Figure 7).

On the other hand, pelagic deposits display well-stratified, continuous, and conformable horizons on seismic profiles. It is sometimes difficult to discriminate between turbiditic and pelagic deposits on seismic profiles because of similarities of seismic facies away from the channel axis. Some contouritic deposits can be observed in places where the seafloor morphology channelizes bottom currents. There, sedimentary layers display strong lateral thickness variations reflecting lateral variations of the bottom current intensity. As a result, the architecture of the contouritic bodies displays a sigmoid shape (Figure 7; Rebesco et al., 2014).

Mass transport deposits originating from the Owen Ridge (Rodriguez et al., 2012) display chaotic to transparent seismic facies, with uneven lobes sometimes identified on the multibeam (Figure 7).

Finally, a particular reflector, with a reverse polarity, is locally observed on seismic profiles on the top of the Owen Ridge, and south of the B3 (Figure 8). This particular reflector may be interpreted as a Bottom Simulating Reflector. Among the various origins proposed for Bottom Simulating Reflectors (Berndt et al., 2004), the diagenetic transformation from smectite to illite may be appropriate considering the context of the Indus distal fan (Shipboard Scientific Party, 1989). In tectonically active areas, Bottom Simulating Reflectors do not necessarily mimic the shape of the seafloor due to local perturbations of the heat flow through fluid circulation within faults (Shedd et al., 2012).

3.3. Stratigraphy

The stratigraphy is constrained from correlation of the seismic lines with ODP Sites (721, 722, and 731) located at the top of the Owen Ridge (Figure 6). These sites document the stratigraphy of the pelagic sediments lying on the Owen Ridge for the last 15 Ma (Figure 6; Rodriguez, Chamot-Rooke, Huchon, Fournier, & Delescluse,

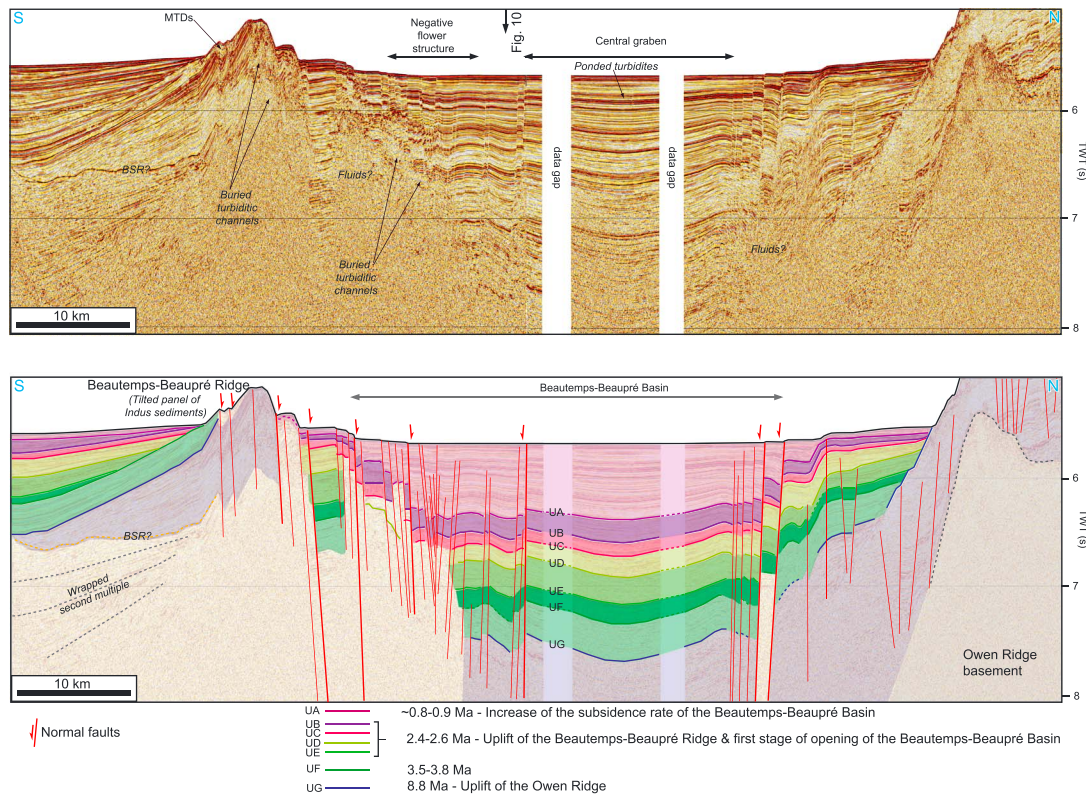


Figure 8. Longitudinal seismic profile crossing the Beautemps-Beaupré Ridge, the Beautemps-Beaupré Basin, and the southern end of the Owen Ridge. UA to UG are the unconformities described in the text. Location of the crossing profile of Figure 10 is indicated. BSR: bottom simulating reflector. See Figure 2b for location.

2014; Shipboard Scientific Party, 1989). There, the pelagic layers sampled at ODP sites have been tied to reflectors of ODP seismic lines collected during the presite survey (Shipboard Scientific Party, 1989). At ODP site 722, the correlation between the geological layers and the seismic reflectors is based on synthetic seismograms built after density log measurements (Shipboard Scientific Party, 1989). The ages are obtained from detailed biostratigraphic studies and the magnetic signature of the sediments, with a time resolution ranging between 0.1 and 1 Ma according to the periods (Shipboard Scientific Party, 1974, 1989). For instance, the reflector dated at 2.4 Ma is very well constrained from biostratigraphic analysis and its peculiar magnetostratigraphic signature, corresponding to the climate change at the beginning of the Pleistocene (Bloemendal & DeMenocal, 1989; Bloemendal et al., 1993). The age of other reflectors can be more ambiguous, like the reflector dated at 3.5–3.8 Ma (Figure 6) based on the sampling of both *Reticulofenestra pseudumbilica* (3.5 Ma) and *Amphirhopalum ypsilon* (3.8 Ma) at the depth corresponding to this reflector (Shipboard Scientific Party, 1974, 1989).

The Owen-2 seismic data set crosses the location of the ODP site 722. The key reflectors previously identified in ODP reports have been simply tied to our new seismic data set, as shown in Figure 6. Despite some local disturbances due to landslides, the correlation of reflectors within the pelagic layers can be easily performed from line to line on the top of the Owen Ridge.

4. Results

4.1. Structure of the Northeastern Part of the Aden-Owen-Carlsberg Triple Junction

4.1.1. Structure of the Beautemps-Beaupré Basin

The structure of the B3 is dominated by normal faulting. All the normal faults are growth faults (i.e., their off-sets increase with depth) whose activity is locally recorded by the fanning configuration of turbidites (Figures 7–12). The normal fault systems form several negative flower structures (Figures 8–10), acting as structural thresholds that affect the distribution of the turbidite infill.

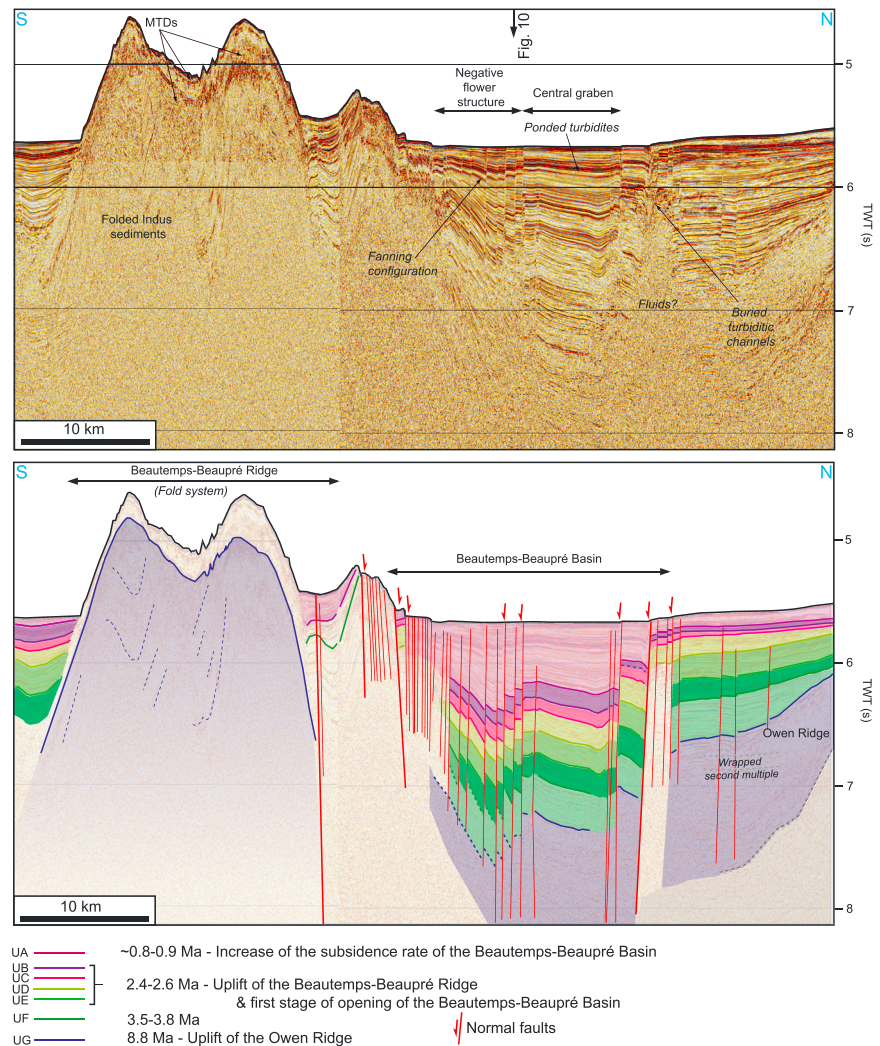


Figure 9. Longitudinal seismic profile crossing the Beautemps-Beaupré Ridge, the Beautemps-Beaupré Basin, and the southern end of the Owen Ridge. UA to UG as on Figure 8. Location of the crossing profile of Figure 9 is shown. MTDs: mass transport deposits. See Figure 2b for location.

4.1.1.1. Longitudinal (S-N) Profiles

The master normal faults bounding the B3 are identified on the longitudinal seismic profiles and have finite vertical offsets reaching ~ 0.25 s (TWT; Figures 8 and 9). At depth, the master faults display chaotic reflections that may correspond to fluid circulation (Figures 8 and 9). The southern part of the basin consists in an \sim E-W trending negative flower structure (Figures 2, 8, and 9). The negative flower structure is the main subsiding area, where the most conspicuous fanning configuration of the turbidites is observed (Figure 9). A central graben is identified between the negative flower structure and the northern boundary of the B3 (Figures 8 and 9). This central graben is ~ 18 -km-wide close to the OFZ (Figure 8) and becomes narrower westward (~ 8 -km-wide on Figure 9).

4.1.1.2. Transverse (SW-NE and W-E) Profiles

On the transverse section (Figure 10), the B3 consists in a series of three synforms dissected by a complex pattern of normal faulting. Here we describe the successive synforms from west to east. The first synform forms an ~ 20 -km-wide subbasin located to the southwest of the main subsiding area of the B3. Northwest dipping faults affect this subbasin. The growth of the faults is well recorded by the fanning configuration of turbidites (Figure 10). The thickness of the sedimentary layers increases toward the center of the synform.

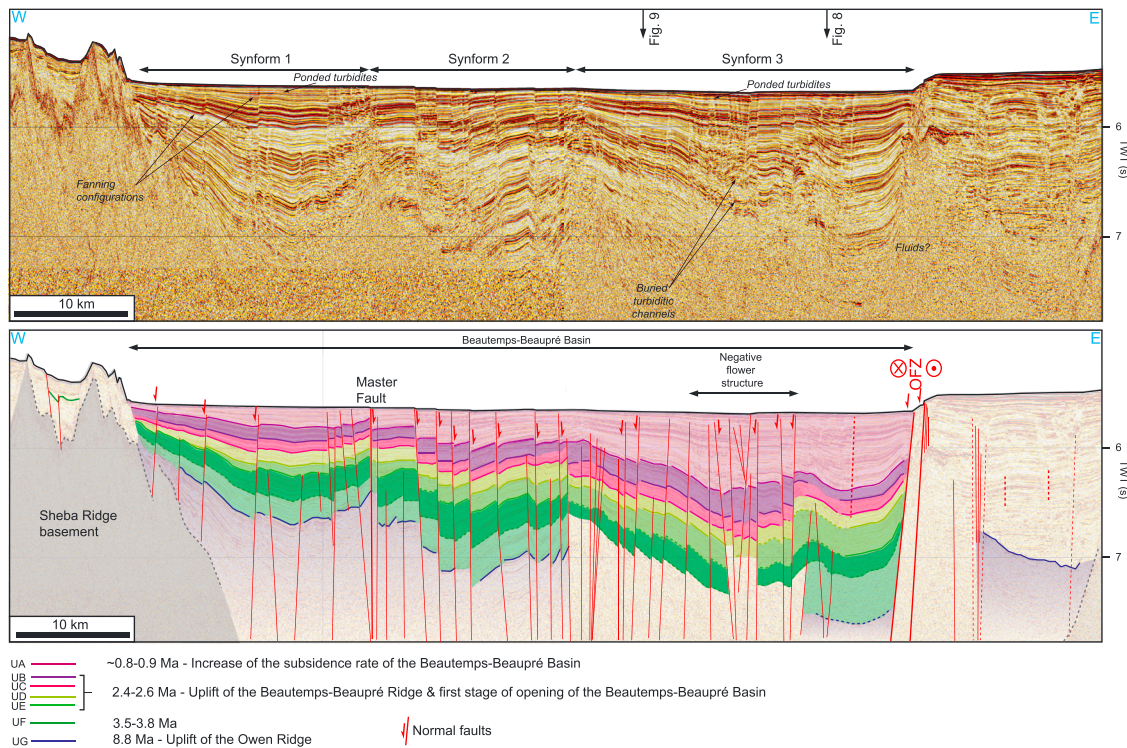


Figure 10. Transverse seismic profile crossing the Beautemps-Beaupré Basin. UA to UG as on Figure 8. Locations of the crossing profiles of Figures 8 and 9 are shown. OFZ: Owen Fracture Zone. See Figure 2b for location.

The main normal fault bounding the southern flank of the B3 (cut obliquely by the profile, Figure 2) constitutes a major structural threshold that marks the transition with the second, ~17-km-wide synform. This structural threshold is characterized by an area of reversal in the fault dip (from west to east; Figure 10). The second synform is asymmetric, with the main area of subsidence (in the uppermost ~0.5 s TWT) located in its western part (Figure 10). On this transverse section (Figure 10), a second structural threshold marks the boundary with the third, ~30-km-wide synform (Figure 10). The latter constitutes the area of maximal subsidence of the B3, with a thickness of the sedimentary infill on the order of 1-s TWT. A negative flower structure demarcates the area of maximal subsidence (Figure 10). Overall, the thickness of the deposits increases toward the flower structure. Finally, this transverse profile reveals that the OFZ is the master fault of the basin, accommodating most of the subsidence (Figure 10).

A second transverse profile (Figure 11) crosscuts the northern tip of the B3, and the southern extremity of the Owen Ridge. There, the B3 is simply expressed as a graben tilted to the west along the OFZ.

4.1.2. Structure of the Beautemps-Beaupré Ridge

The B3 is bounded to the south by a series of SW-NE trending, up to 750-m-high bathymetric ridges hereafter referred as the Beautemps-Beaupré Ridge (Figure 2). Seismic profiles reveal the Beautemps-Beaupré Ridge is a fold system deforming turbidites from the Indus fan (Figures 8, 9, and 12). On the profile close to the OFZ (Figure 8), the Beautemps-Beaupré Ridge appears as a tilted panel of Indus sediments (Figures 8 and 12). To the west, in Figure 9, the Beautemps-Beaupré Ridge consists of a fold system composed of three antiforms and two synforms. There, large mass transport deposits are trapped within the synform domains (Figure 9). Some north dipping normal faults observed on both the multibeam (Figure 2) and the seismic profiles crosscut the fold system (Figures 8 and 9). These normal faults are related to the opening of the B3.

4.1.3. Identification of a Beautemps-Beaupré Fracture Zone

A strike slip fault system is observed on the multibeam between the Owen Transform and the OFZ (Figure 13). It is hereafter mentioned as the "Beautemps-Beaupré Fracture Zone." These traces of strike-slip tectonics are encountered in places where turbidite sedimentation shifted to pelagic sedimentation, allowing a good

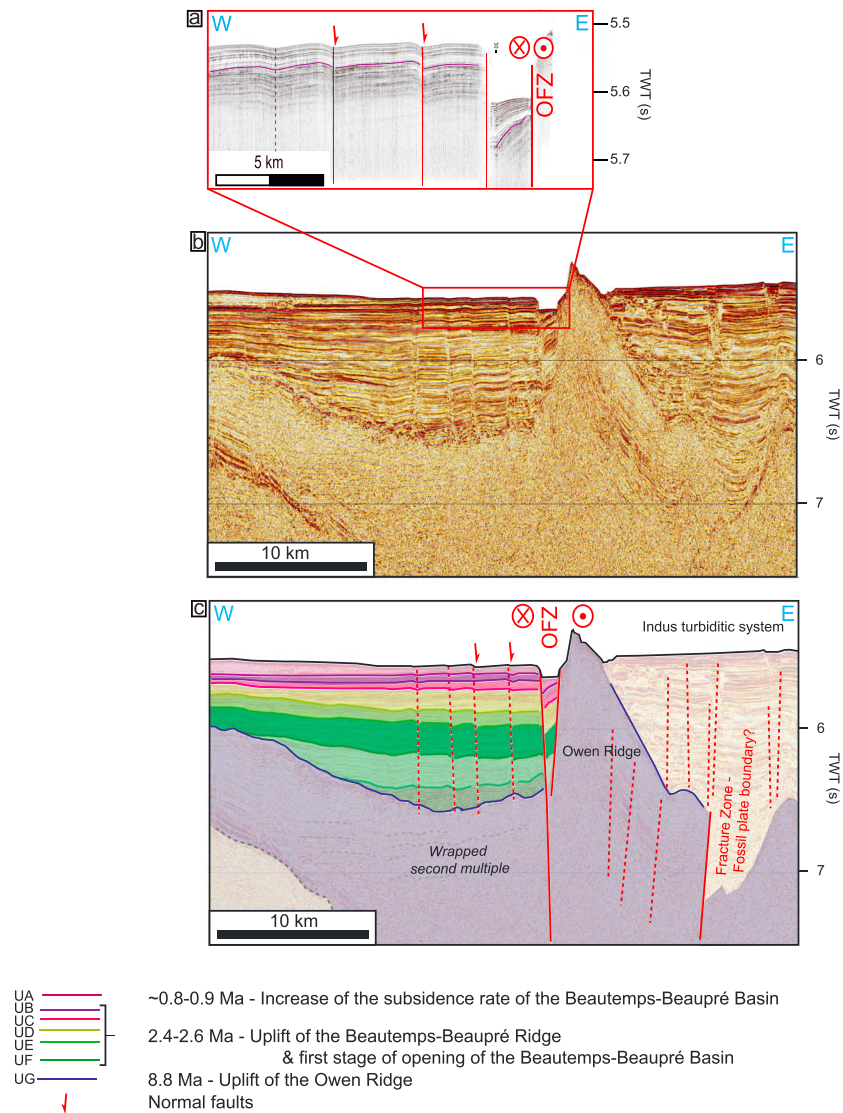


Figure 11. Transverse seismic profile: (b) data and (c) interpretation, crossing the northern end of the Beautemps-Beaupré Basin, the Owen Fracture Zone, and the southern end of the Owen Ridge. Figure 10a is a 3.5 kHz profile of part of the profile. UA to UG as in Figure 8. OFZ: Owen Fracture Zone. See Figure 2b for location.

preservation of the morphology on the seafloor. This strike slip fault system is composed of two 120-km-long and 65-km-long main segments, separated by one major bend at $\sim 14^{\circ}\text{N}$ (Figure 12). The southern segment consists of an en-échelon fault system composed of SW-NE trending splays (Figure 13). Several small-scale pressure ridges and pull-apart basins are observed along the bend (Figure 13). The northern segment displays a very simple, linear fault structure. This strike-slip system is not associated with any recorded seismicity.

4.2. Tectono-Stratigraphic Framework

4.2.1. The Significance of the Angular Unconformities

Interactions between tectonics and the dynamics of the Indus turbiditic system result in a complex succession of angular unconformities observed along the borders of the B3 and on the southern flank of the Beautemps-Beaupré Ridge (Figures 8–12). Investigating the significance of these unconformities raises numerous difficulties.

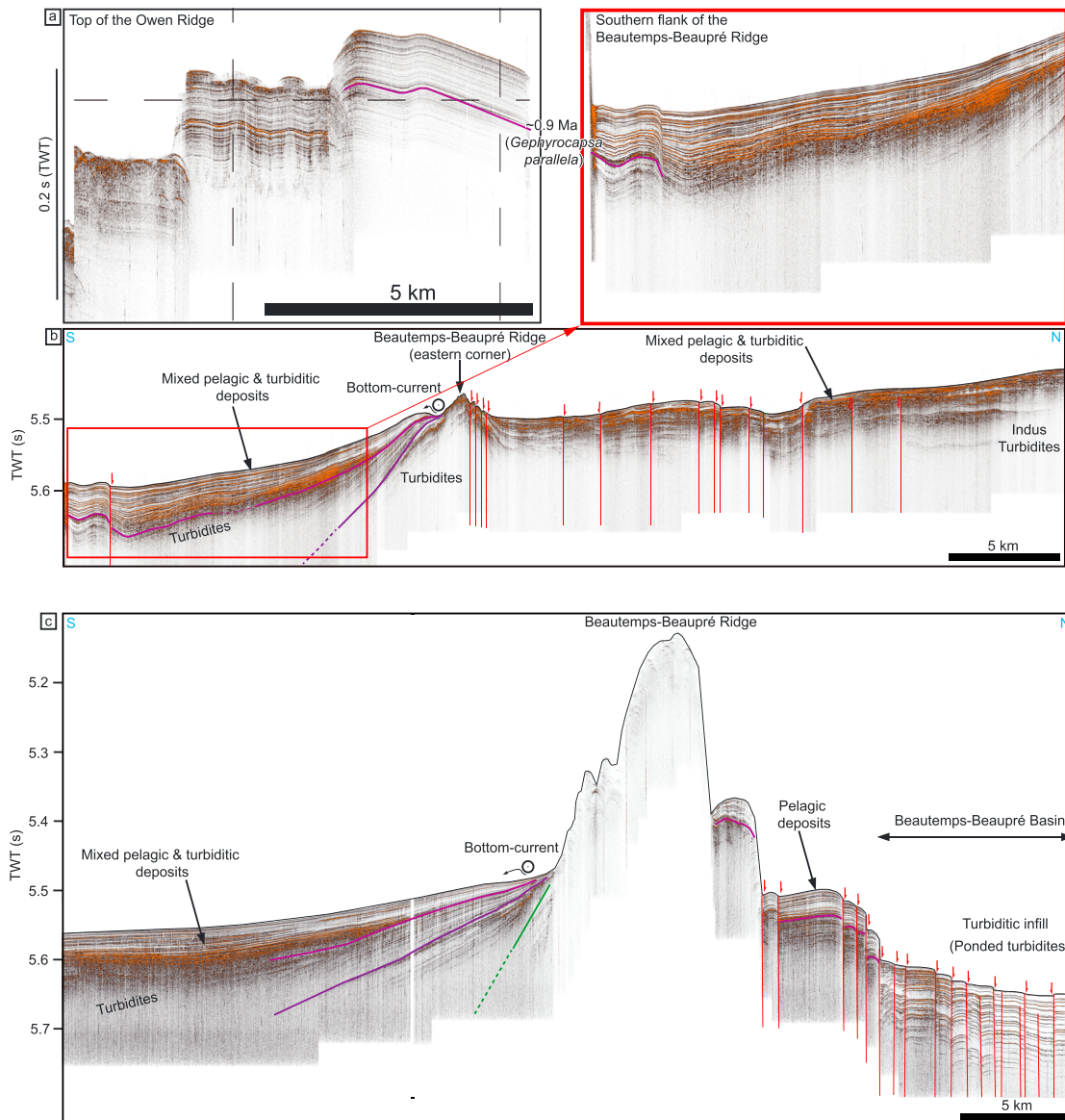


Figure 12. (a) Correlation of a subbottom profile at the top of the Owen ridge with a profile on the southern flank of the Beautemps-Beaupré Ridge (inset of figure b). (b and c) Subbottom profiles (3.5 kHz) crossing the Beautemps-Beaupré Basin and Ridge. See the bold lines on Figure 2b for location.

1. First, it is difficult to discriminate whether the angular unconformities at the edge of active structures reflect tectonic changes (e.g., opening of a basin or uplift of a ridge, changes in subsidence or uplift rates, and changes in fault slip rates) or changes in the sedimentary record of the deformation (i.e., changes in the dynamics of the Indus turbidite fan in response to avulsion processes and/or climatic and sea level changes (Bourget et al., 2013; Clift et al., 2001, 2008, 2014; Rodriguez et al., 2011, 2013).
2. Second, the opening of the B3 is not clearly recorded by any remarkable unconformity within the core of the basin, which displays conformable reflectors in most areas (Figures 8, 9, and 10). The similar configuration of the numerous unconformities (either related to tectonic or sedimentary processes) makes it difficult to discriminate which one marks the opening of the B3. The onset of fanning configuration of the turbidite infill is an ambiguous marker of the onset of normal fault activity because the basin emplaced in an area that also recorded the uplift of the Owen Ridge (Rodriguez, Chamot-Rooke, Huchon, Fournier, and Delescluse, 2014).

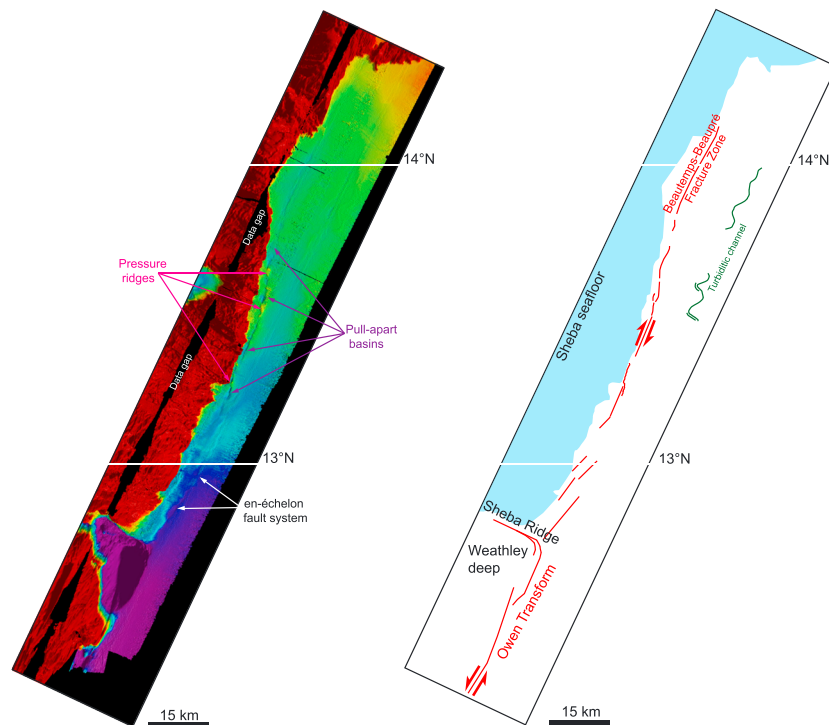


Figure 13. Multibeam bathymetry of the Beautemps-Beaupré Fracture Zone, and the interpreted structure (see Figure 1b for location).

- Third, the evolution of the AOC triple junction spans periods where sedimentation rates were much greater than fault slip rates. Larger sedimentation rates are not a priori favorable for accurate fault activity record, and for identification of the reflector marking their emplacement, because they permanently flood the fault scarp (Barnes & Pondard, 2010; Pondard & Barnes, 2010).

All these difficulties can, however, be overcome from the detailed structural analysis of the area and correlation of the profiles with drilling sites located on the top of the Owen Ridge (Figures 14a and 14b).

4.2.2. Ties of Seismic Lines Crossing the Beautemps-Beaupré Basin and Ridge With ODP Sites Located at the Top of the Owen Ridge

The sedimentary series that record the uplift of the southern side of the Beautemps-Beaupré Ridge consists of a succession of turbidites and pelagites (Figures 14a and 14b). Some unconformities result from the progressive shift from turbidite to pelagite along the uplifted panel, which occurs in areas gradually uplifted above the level of turbidite deposition. Other unconformities (e.g., UF) result from the pelagic layers that are progressively buried by increased turbidite sedimentation catching-up the uplifted seafloor (Figure 14b).

Consequently, a sequence of pelagites has been isolated on the top of the Beautemps-Beaupré Ridge since seafloor uplift began in this area. This series of pelagites can be fairly correlated with the pelagic series on the top of the Owen Ridge, based on the striking similarity of the amplitude pattern of the reflectors (Figure 14). Figure 14 displays side by side enlargements of the seismic profiles from the southern side of the Beautemps-Beaupré Ridge and the top of the Owen Ridge. This correlation provides valuable stratigraphic constraints from 8.8 Ma (i.e., the onset of the Owen Ridge uplift; Rodriguez, Chamot-Rooke, Huchon, Fournier, and Delescluse, 2014), to 2.5–2.6 Ma.

The sediments varying in age from recent to 2.5–2.6 Ma on the southern flank of the Beautemps-Beaupré Ridge display a fanning configuration. The fanning pattern is mainly formed by turbidites (but the resolution of seismic data set makes it difficult to precisely discriminate the pelagic layers among the turbiditic ones; Figures 8 and 14b). Fortunately, the subbottom profiles provide a better imaging of the sedimentary series for the top of the fanning sequence and allow us to safely identify the pelagic intervals (Figure 12). Figure 12a displays a side-by-side view of a 3.5 kHz profile collected along the southern flank of the

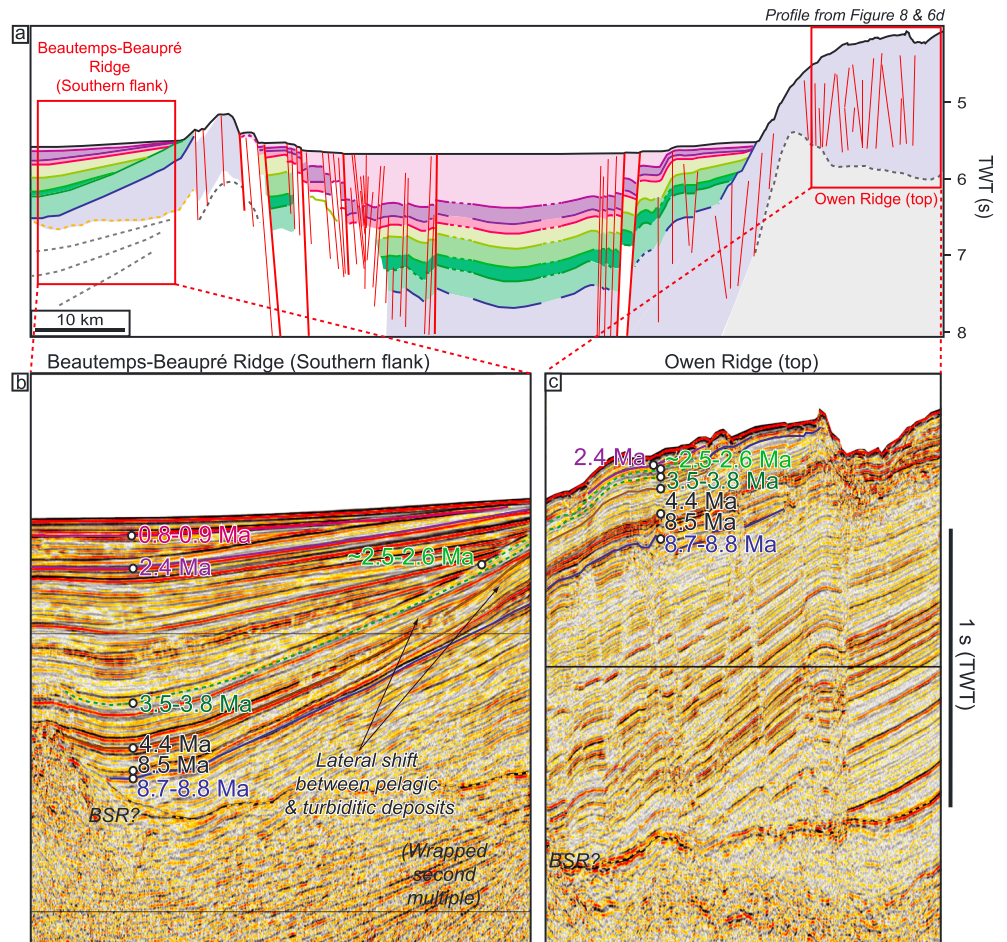


Figure 14. Ages assigned to the stratigraphic sequence of the Beautemps-Beaupré Basin and Ridge system. (a) Line drawing of the profile displayed in Figure 8, showing the location of the segments used to build the first part of the stratigraphic framework (southern Beautemps-Beaupré Ridge). (b) Side-by-side view of a segment of the profile from the southern flank of the Beautemps-Beaupré Ridge and (c) a segment of the profile from the top of the Owen Ridge. Note the similarity of the pelagic sequences between both locations. (d) Line drawing of the profile displayed in Figure 8, showing the location of the segments used to build the second part of the stratigraphy (correlation of the southern part of the basin with its northern part). (e) Side-by-side view of a segment of the profile at the northern border of the Beautemps-Beaupré Basin and (f) the segment from the southern flank of the Beautemps-Beaupré Ridge, highlighting the similarities between the sedimentary sequences. BSR: bottom simulating reflector.

Beautemps-Beaupré Ridge and one collected at the top of the Owen Ridge. Although bottom currents locally induce lateral thickness variations of the pelagic layers on the southern side of the Beautemps-Beaupré Ridge (Figure 12), the pelagic series can be fairly correlated with the ones imaged by subbottom profiles at the top of the Owen Ridge, close to the location of the ODP Sites (Figure 6). Here again, the correlation is based on the amplitude pattern of the reflectors on subbottom profiles. The uppermost transition from turbidites to pelagites observed south of the Beautemps-Beaupré Ridge is dated at ~0.8–0.9 Ma (Figure 12). This age is consistent with the age of the last unconformity recorded within the Indus fan at ODP Site 720, estimated at 0.75–0.8 Ma (Shipboard Scientific Party, 1989). It corresponds to a major episode of avulsion of the Indus turbiditic system, recognized all along the strike of the OFZ (Rodríguez et al., 2011). A second, deeper unconformity corresponding to a shift from turbidites to pelagites can be dated at ~2.4 Ma from the correlation of the sequence of reflectors with that from the top of the Owen Ridge (Figure 12a).

The combined seismic stratigraphy worked-out from these correlations is shown in Figure 14. Figures 14d–14f present a side-by-side view of a seismic section from the Beautemps-Beaupré Ridge and a seismic section

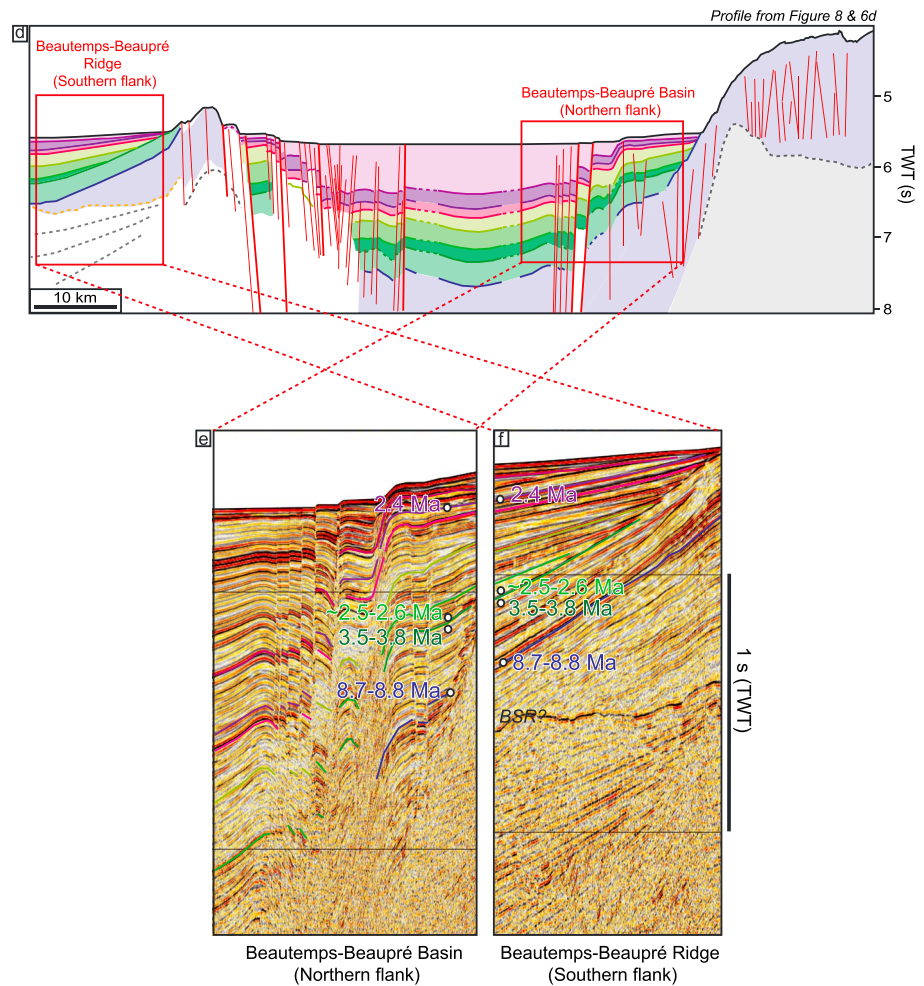


Figure 14. (continued)

from the northern edge of the B3. Figures 14e and 14f highlight a similar succession of unconformities in both areas. The numerous angular unconformities identified on the southern limb of the Beautemps-Beaupré Ridge can be fairly correlated from line to line with the angular unconformities observed on the northern border of the B3 (Figures 14e and 14f).

4.3. Significance of the Angular Unconformities, Relative Chronology, and Age Estimates of the Deformation

4.3.1. Sequence Sealed by the 8.7–8.8-Myr-Old Unconformity (Labeled UG):

The oldest dated key horizon is the unconformity corresponding to the uplift of the Owen Ridge (labeled UG; Figures 8–11). In the northern part of the B3, the unconformity is marked by onlap terminations of the Indus turbidites over the mass transport deposits resulting from landslides triggered subsequent to the uplift of the Owen Ridge (Figure 8; Rodriguez et al., 2012; Rodriguez, Chamot-Rooke, Huchon, Fournier, & Delescluse, 2014). This unconformity can be identified almost continuously within the B3 (Figures 8–11). On the southern side of the Beautemps-Beaupré Ridge, the unconformity UG marking the onset of uplift is dated at 8.8 Ma (Figures 8 and 14b). It corresponds to the first unconformity characterized by the lateral shift from turbidites to pelagites. The record of the southern flank of the Beautemps-Beaupré Ridge provides a more precise age of the onset of uplift of the Owen Ridge at 8.7–8.8 Ma, compared to previous age estimated bracketed between 8.2 and 8.8 Ma (Rodriguez, Chamot-Rooke, Huchon, Fournier, & Delescluse, 2014).

The sedimentary sequence beneath the 8.7–8.8-Myr-old unconformity displays some traces of turbidite current channel axis in the part of the Beautemps-Beaupré Ridge affected by normal faulting and eroded at the

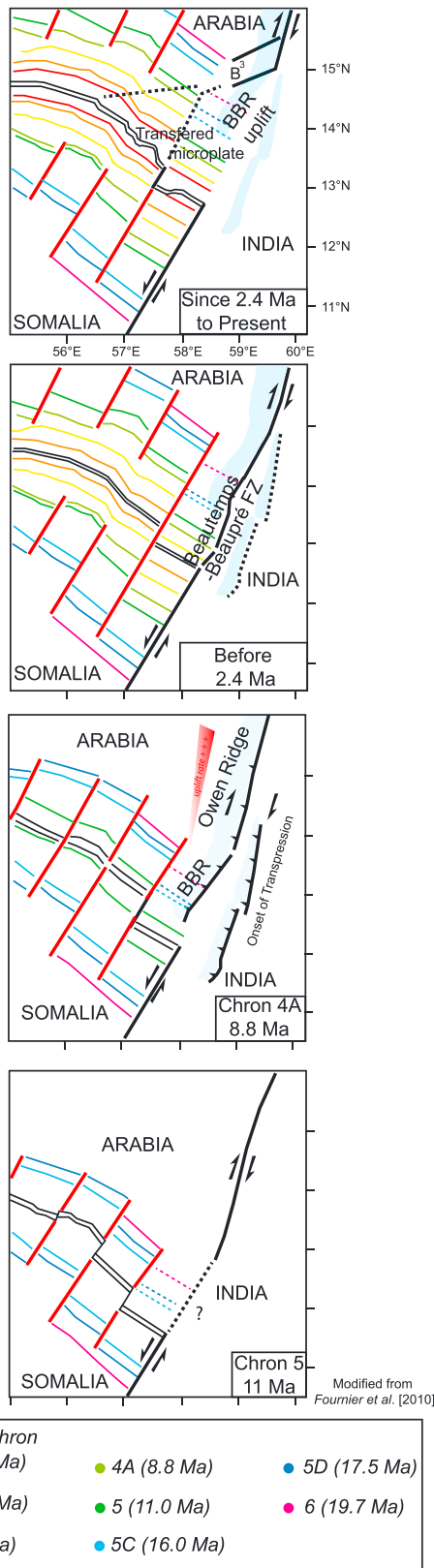


Figure 15. Reconstructed evolution of the Aden-Owen-Carlsberg triple junction since 11 Ma. Modified from Fournier et al. (2010). See the discussion for detailed comments.

top of the Beaufort-Beaufort Ridge (Figure 8). This sequence is tilted toward the Owen Ridge, which indicates that it was not uplifting at that time (Figures 8 and 14b). The minor angular unconformities observed within this sequence can be interpreted either as the result of the sedimentary levees of the turbidite channels, or the result of nearby active tectonics.

4.3.2. The 8.7 to 2.5–2.6-Myr-Old Unconformities (Between UG and UF): Record of the Progressive Uplift of the Owen Ridge

These unconformities are only observed in the southern flank of the Beaufort-Beaufort Ridge (Figures 8 and 14). They correspond to lateral shifts of sedimentation (from turbidite to pelagite) in response to the progressive uplift of the Owen Ridge. The succession of several of these unconformities during the 8.7–2.5 Ma interval indicates a tight competition between seafloor uplift in this area (edge of the Owen Ridge) and the turbiditic sedimentation.

4.3.3. The 2.6–2.4-Myr-Old Unconformities: Increase in the Indus Sedimentation Rates, Major Uplift of the Beaufort-Beaufort Ridge, and Opening of the Beaufort-Beaufort Basin.

According to our proposed stratigraphy, all the angular unconformities from UE to UB (Figures 8–11 and 14) were formed in a very short time interval of 0.1–0.2 Ma, between 2.4 and 2.5–2.6 Ma. This interval corresponds to a pulse of turbidites, with rates >1.5 km/Ma south of the Beaufort-Beaufort Ridge (Figures 8 and 9). This pulse of turbidites may have been triggered by the coeval episode of intensification of the Indian monsoon (An et al., 2001; Clift et al., 2008). The 2.5- to 2.6-Myr-old unconformity (UF) displays the same dip as all the layers lying underneath, indicating that all the sequences deposited prior to 2.5–2.6 Ma have been tilted as a single panel during the same event. Moreover, the angle between UF and the onlap UE is the largest among all the observed unconformities (Figures 8 and 14). This unconformity UF therefore indicates abrupt tilting shortly after 2.5–2.6 Ma. This reflector UF also marks the base of the fanning configuration of the sediments at the western edge of the B3 (transverse profile; Figure 10). However, in the inner parts of the basin, the sedimentary units overlying the reflector UF do not show the expected thickening between the borders and the core of the basin. These units also locally display some remnants of turbidite current channels, observed on several seismic lines (Figures 9 and 10), which is not consistent with a deep basin. The sedimentation rates were probably so high that turbidites totally flooded the incipient basin.

4.3.4. Since 2.4 Ma: Subsidence of the Beaufort-Beaufort Basin

The units above the unconformity UB clearly show the deepening of the B3, at a mean rate of ~500 m/Ma since 0.8–0.9 Ma in the area of maximal subsidence (Figures 8 and 10). These units cap the youngest turbidite current channel within the basin and are composed of ponded turbidites captured by the basin (Figures 8–12). These units also clearly display the fanning configuration of the turbidites at the edge of the normal faults.

5. Discussion

5.1. Detailed Reconstruction of the Evolution of the Aden-Owen-Carlsberg Triple Junction

The new tectonic evolution of the AOC triple junction deduced from the analysis of the seismic data set is summarized in Figure 15.

The precise configuration of the triple junction prior to 11 Ma remains unknown. We assume that the triple junction had a Ridge-Fault-Fault configuration, although evidences for the prolongation of the Owen Transform are scarce.

The seismic data set in the vicinity of the B3 confirms the onset of the uplift of the Owen Ridge at 8.7–8.8 Ma as previously proposed by Rodriguez, Chamot-Rooke, Huchon, Fournier, and Delescluse (2014) and Rodriguez, Chamot-Rooke, Huchon, Fournier, Lallemand, et al. (2014). The Owen Ridge uplift is recorded at the Beautemps-Beaupré Ridge. The timing and mode of uplift of the transverse ridges identified east of the B3, including the Varun Bank (Figure 3), remain unclear because of the lack of available seismic data. Either the Varun Bank reflects the diffuse configuration of the plate boundary at the time of the uplift of the Owen Ridge, or it constitutes a remnant of an older, pre-Miocene geological event related to the complex dynamics of the India-Arabia plate boundary (Rodriguez et al., 2016).

The timing of emplacement of the Beautemps-Beaupré Fracture Zone identified in this study (Figure 13) is difficult to constrain. The vintage profile in Figure 3 shows offset of recent, uppermost reflectors of the section. The shift to pelagic deposition has preserved the seafloor signature of the fault, even after its deactivation, as observed elsewhere along the OFZ (Rodriguez et al., 2011). The seafloor signature of the Beautemps-Beaupré Fracture Zone would have been erased by the pulse of turbidites recorded at 2.4–2.5 Ma. This fault-system was probably still active during this detritic pulse, and deactivated soon after, when the B3 opened 2.4 Ma. This fault system is interpreted as a transient stage active between the end of the uplift of the Owen Ridge and the opening of the B3. We consider this structure as a short-lived strike-slip fault (Figure 14).

The uplift of the Beautemps-Beaupré Ridge then started at 2.5–2.6 Ma, followed soon after by the emplacement of the B3 at 2.4 Ma. During its first stage of opening, the B3 was not deep enough to significantly affect the behavior of the distal Indus fan, characterized by huge sedimentation rates at that time. During this time span, the Indus fan has continued to develop turbidite current channels despite the incipient normal fault systems related to the opening of the basin. A major episode of subsidence of the basin occurred at 0.8–0.9 Ma.

The major outcome of this new tectono-stratigraphic framework is the emplacement of the present-day configuration of the AOC triple junction at 2.4 Ma and not in the Late Miocene as previously inferred (Fournier et al., 2010). Considering that the 10–12 km morphological offsets of the OFZ were formed during the last 2.4 Myr implies a revised dextral rate of India-Arabia relative motion at $\sim 4.2\text{--}5$ mm/year.

5.2. Mode of Opening of the Beautemps-Beaupré Basin

The 120-km-long, 50-km-wide B3 opened in only 2.4 Ma, which corresponds to 10–12 km of dextral offset along the OFZ. In contrast with other oceanic pull-apart basins (for instance, the Cayman Trough in the Caribbean; Hayman et al., 2011; or pull-apart basins along the Blanco Transform in the Pacific; Embley & Wilson, 1992), the mode of opening of the B3 cannot be explained by a continuous growth of the basin with increasing relative motion (Aydin & Nur, 1982; Mann, 2007; Mann et al., 1983). The size of the B3 may be explained by the isolation of a large ~ 110 -km-long subsiding block, subsequently affected by 10–12-km of distributed extension (Figure 16). The formation of a half graben involves a 3-block system, where the subsiding block is bounded by a main normal fault and its antithetic, which is consistent with analog models (Brun & Mauduit, 2008). The main bounding fault induced the uplift of the Beautemps-Beaupré Ridge. The distance between the main normal fault and its antithetic defines the dimensions of the subsiding block. Because the B3 emplaced at the southern termination of the OFZ, the structure shares similarities with horsetail structures; that is, oblique fault splays rooting on the main strike-slip fault on one side, and a loosely defined boundary on the other side (Figure 16). The turbiditic infill has smoothed the seafloor signature of the splays, which makes difficult the reconstruction of their precise arrangement. A limit of our data set, and hence of this model of opening, is the lack of identification of any décollement layer at depth, supporting the opening of the pull-apart basin. Shales within the Indus fan may act as potential décollement levels (Calvès et al., 2008), but it is also possible that the décollement roots within the basement.

The subsidence related to the opening of the B3 is on the order of 1.2 km according to our interpretation (Figure 8). This value is less than the ~ 3 km expected from modeling of the gravity field (Figure 4; Fournier, Chamot-Rooke, et al., 2008; Fournier, Petit, et al., 2008). Therefore, an episode of extension might have

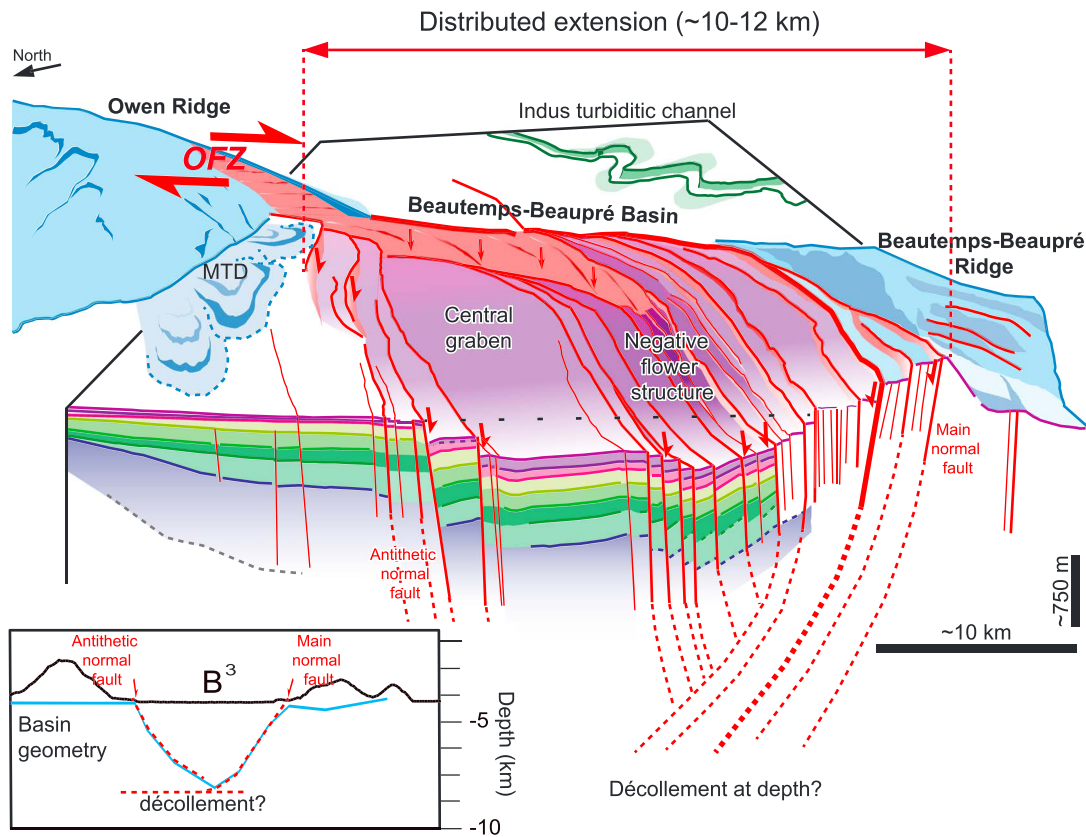


Figure 16. Isometric 3-D view of the structure of the Beautemps-Beaupré Basin, highlighting its mode of opening as a fault termination basin at the end of the OFZ.

affected the basement prior to the opening of the B3. The origin and the timing of such episode are unknown. No such gravity anomaly is identified along the oceanic seafloor formed at the Sheba spreading center (Fournier, Chamot-Rooke, et al., 2008; Fournier, Petit, et al., 2008). It may be tentatively related to a previous episode of pull-apart basin formation along the India-Arabia plate boundary. The gravity field indicates that this hypothetical episode formed a heterogeneity in the basement, which may have controlled the location of the southern termination of the OFZ during the reorganization of the system 2.4 Ma.

A similar mode of opening has been proposed for the 20°N pull-apart Basin and the Dalrymple Trough along the OFZ (Rodriguez et al., 2013; Rodriguez, Chamot-Rooke, Huchon, Fournier, Lallemand, et al., 2014). The isolation of a subsiding block bounded by conjugate normal fault has also been commonly invoked to explain the narrowness of pull-apart basins or some continental rifts (Dead Sea pull-apart basin, Brun & Gutscher, 1992; Corinth Rift, Lambotte et al., 2014; ten Brink & Ben-Avraham, 1989; ten Brink & Flores, 2012; and Rhine graben).

5.3. Do the Successive Reorganizations of the Aden-Owen-Carlsberg Triple Junction Mark a Series of Kinematic Changes?

The 8.8 Ma change in configuration of the AOC triple junction is coeval with the last major kinematic change affecting the Indian Ocean around 8 Ma. Kinematics studies at the scale of the Indian Ocean do not document any significant kinematic change for the last 5.2 Ma (DeMets et al., 2017; DeMets & Merkouriev, 2016). Even if the precise kinematics of Arabia for the last 3.14 Ma remain to be constrained (Fournier et al., 2010), these kinematic reconstructions are locally constrained by the magnetic chron 1n at 0.78 Ma. In the lack of any detected kinematic change, the driver of the 2.4 Ma reorganization of the entire India-Arabia boundary, from the AOC triple junction to the Makran subduction zone (Rodriguez et al., 2014), is unclear.

One may consider that the successive changes in configuration of the AOC triple junction simply reflect a series of transient adjustments since ~8 Ma unrelated to kinematic changes, as observed for many triple junctions (Ligi et al., 1999). However, some processes at the origin of slight changes in the stress field may be considered as potential drivers of the formation of the OFZ and the reorganization of the AOC triple junction at 2.4 Ma. A possible driver may be the accretion of oceanic crust along the northern segments of the Red Sea between 2–3 Ma (Thetis and Nereus segments; Ligi et al., 2011, 2012, 2018), a period when intense mantle upwelling is expected, which may have potentially affected the stress field of Arabia as far as its eastern boundary. Another possible driver may be the 2.4 Ma major monsoon intensification (An et al., 2001). Variations in sedimentation rates within the Indus fan in response to a monsoon intensification can affect the load applied on the plate boundary, as well as the heat flux, and therefore the distribution of stress and friction along the fault. The intensification of the monsoon may have also affected the force balance at the Himalayan belt (Iaffaldano et al., 2006, 2011; Molnar & Stock, 2009).

Because all these potential drivers are extremely difficult to quantify, the origin of the abrupt reorganization of the India-Arabia plate boundary at 2.4 Ma in the lack of any significant kinematic change remains an opened question.

6. Conclusions

The seismic data set documents successive transient episodes of reorganization of the AOC triple junction since the last major kinematic change ~8 Ma that triggered the uplift of the Owen Ridge. The present-day configuration of the AOC triple junction emplaced only 2.4 Ma, coevally with a structural reorganization of the entire India-Arabia plate boundary up to the Makran subduction zone. This spectacular structural reorganization, recognized over more than 800 km, is not related to any remarkable kinematic change and might find its driver in slight changes of forces applied on the fault system.

Acknowledgments

We thank officers and crew members of the Beautemps-Beaupré vessel for their help in data acquisition during AOC and OWEN 1-2 cruises, as well as the GENAVIR team. Processing of the Owen-2 data set was carried out using the CCG GEOVATION software. The data set may be accessible on personal demand at rodriguez@geologie.ens.fr. Information about the access to data on which this work is based can further be found using the following DOIs: <https://doi.org/10.17600/6090030> (AOC cruise), <https://doi.org/10.17600/9090020> (OWEN cruise), and <https://doi.org/10.17600/12090050> (OWEN2 cruise). This study was supported by SHOM, IFREMER, INSU-CNRS. We sincerely thank N. Mitchel, M. Ligi, and A. Schettino for their constructive and detailed reviews.

References

- An, Z., Kutzbach, J. E., Prell, W. L., & Porter, S. C. (2001). Evolution of Asian monsoons and phased uplift of the Himalaya–Tibetan plateau since late Miocene times. *Nature*, *411*, 62–66.
- Andersen O., Knudsen, P., Kenyon, S., Factor, J., & Holmes, S. (2013). The dtu13 global marine gravity field—First evaluation. Technical report, DTU Space - National Space Institute
- Aydin, A., & Nur, A. (1982). Evolution of pull-apart basins and their scale independence. *Tectonics*, *1*, 91–105. <https://doi.org/10.1029/TC001i001p00091>
- Barnes, P., & Pondard, N. (2010). Derivation of direct on-fault submarine paleoearthquake records from high-resolution seismic reflection profiles: Example from the Wairau Fault, New Zealand. *Geochemistry, Geophysics, Geosystems*, *11*, Q11013. <https://doi.org/10.1029/2010GC003254>
- Berndt, C., Büinz, S., Clayton, T., Mienert, J., & Saunders, M. (2004). Seismic character of bottom simulating reflectors: Examples from the mid-Norwegian margin. *Marine and Petroleum Geology*, *21*(6), 723–733. <https://doi.org/10.1016/j.marpetgeo.2004.02.003>
- Bird, R. T., Naar, D. F., Larson, R. L., Searle, R. C., & Scotese, C. (1998). Plate tectonic reconstructions of the Juan Fernandez microplate: Transformation from internal shear to rigid rotation. *Journal of Geophysical Research*, *103*, 7049–7067. <https://doi.org/10.1029/97JB02133>
- Bloemendal, J., King, J. W., Hunt, A., DeMenocal, P. B., & Hayashida, A. (1993). Origin of the sedimentary magnetic record at Ocean Drilling Program Sites on the Owen Ridge, Western Arabian Sea. *Journal of Geophysical Research*, *98*, 4199–4219. <https://doi.org/10.1029/92JB02914>
- Bloemendal, J., & DeMenocal, P. B. (1989). Evidence for a change in the periodicity of tropical climate cycles at 2.4 Myr from whole-core magnetic susceptibility measurements. *Nature*, *342*(6252), 897–900. <https://doi.org/10.1038/342897a0>
- Bonatti, E., Brunelli, D., Buck, W. R., Cipriani, A., Fabretti, P., Ferrante, V., et al. (2005). Flexural uplift of a lithospheric slab near the Vema transform (central Atlantic): Timing and mechanisms. *Earth and Planetary Science Letters*, *240*(3–4), 642–655. <https://doi.org/10.1016/j.epsl.2005.10.010>
- Bourget, J., Zaragosi, S., Rodriguez, M., Fournier, M., Garland, T., & Chamot-Rooke, N. (2013). Late Quaternary megaturbidites from the Indus fan : Origin and stratigraphic significance. *Marine Geology*, *336*, 10–23. <https://doi.org/10.1016/j.margeo.2012.11.011>
- Brun, J. P., & Gutscher, M.-A. (1992). Deep crustal structure of the Rhine Graben from DEKORP-ECORS seismic reflection data: A summary. *Tectonophysics*, *208*(1–3), 139–147. [https://doi.org/10.1016/0040-1951\(92\)90340-C](https://doi.org/10.1016/0040-1951(92)90340-C)
- Brun, J.-P., & Mauduit, O. (2008). Rollovers in salt tectonics: The inadequacy of the listric fault model. *Tectonophysics*, *457*(1–2), 1–11. <https://doi.org/10.1016/j.tecto.2007.11.038>
- Bull, J. M., DeMets, C., Krishna, K. S., Sanderson, D. J., & Merkouriev, S. (2010). Reconciling plate kinematic and seismic estimates of lithospheric convergence in the central Indian Ocean. *Geology*, *38*(4), 307–310. <https://doi.org/10.1130/G30521.1>
- Bull, J. M., & Scrutton, R. A. (1990). Fault reactivation in the central Indian Ocean and the rheology of oceanic lithosphere. *Nature*, *344*(6269), 855–858. <https://doi.org/10.1038/344855a0>
- Bull, J. M., & Scrutton, R. A. (1992). Seismic reflection images of intraplate deformation, Central Indian Ocean, and their tectonic significance. *Journal of the Geological Society*, *149*(6), 955–966. <https://doi.org/10.1144/gsjgs.149.6.0955>
- Calvès, G., Huuse, M., Schwab, A., & Clift, P. (2008). Three-dimensional seismic analysis of high-amplitude anomalies in the shallow subsurface of the Northern Indus Fan: Sedimentary and/or fluid origin. *Journal of Geophysical Research*, *113*, B11103. <https://doi.org/10.1029/2008JB005666>

- Chamot-Rooke, N., Fournier, M., & Scientific Team of AOC and OWEN Cruises (2009). Tracking Arabia-India motion from Miocene to Present. American Geophysical Union, Fall Meeting 2009.
- Chamot-Rooke, N., Jestin, F., & DeVoogd, B. (1993). Intraplate shortening in the central Indian-ocean determined from a 2100-km-long north-south deep seismic-reflection profile. *Geology*, *21*(11), 1043–1046. [https://doi.org/10.1130/0091-7613\(1993\)021%3C1043:ISITC%3E2.3.CO;2](https://doi.org/10.1130/0091-7613(1993)021%3C1043:ISITC%3E2.3.CO;2)
- Clift, P. D., Giosan, L., Henstock, T. J., & Tabrez, A. R. (2014). Sediment storage and reworking on the shelf and in the Canyon of the Indus River-Fan system since the last glacial maximum. *Basic Research*, *26*(1), 183–202. <https://doi.org/10.1111/bre/12041>
- Clift, P. D., Hodges, K. V., Heslop, D., Hannigan, R., Van Long, H., & Calvès, G. (2008). Correlation of Himalayan exhumation rates and Asian monsoon intensity. *Nature Geoscience*, *1*(12), 875–880. <https://doi.org/10.1038/ngeo351>
- Clift, P. D., Shimizu, N., Layne, G. D., Blusztain, J. S., Gaedicke, C., Schluter, H. U., et al. (2001). Development of the Indus Fan and its significance for the erosional history of the Western Himalaya and Karakoram. *Geological Society of America Bulletin*, *113*(8), 1039–1051. [https://doi.org/10.1130/0016-7606\(2001\)113%3C1039:DOTIFA%3E2.0.CO;2](https://doi.org/10.1130/0016-7606(2001)113%3C1039:DOTIFA%3E2.0.CO;2)
- Cochran, J. (1978). Vema cruise V3502. <https://doi.org/10.7284/906184>
- Cronin, V. S. (1992). Types and kinematic stability of triple junctions. *Tectonophysics*, *207*, 287–301. [https://doi.org/10.1016/0040-1951\(92\)90391-I](https://doi.org/10.1016/0040-1951(92)90391-I)
- d'Acremont, E., Leroy, S., Beslier, M.-O., Bellahsen, N., Fournier, M., Robin, C., et al. (2006). Structure and evolution of the eastern Gulf of Aden conjugate margins from seismic reflection data. *Geophysical Journal International*, *160*, 869–890. <https://doi.org/10.1111/j.1365-246X.2005.02524.x>
- d'Acremont, E., Leroy, S., Maia, M., Gente, P., & Autin, J. (2010). Volcanism, jump and propagation on the Sheba Ridge, eastern Gulf of Aden: Segmentation evolution and implications for oceanic accretion processes. *Geophysical Journal International*, *180*, 535–551. <https://doi.org/10.1111/j.1365-246X.2009.04448.x>
- Delescluse, M., & Chamot-Rooke, N. (2007). Instantaneous deformation and kinematics of the India-Australia Plate. *Geophysical Journal International*, *168*(2), 818–842. <https://doi.org/10.1111/j.1365-246X.2006.03181.x>
- Delescluse, M., Montési, L. G. J., & Chamot-Rooke, N. (2008). Fault reactivation and selective abandonment in the oceanic lithosphere. *Geophysical Research Letters*, *35*, L16312. <https://doi.org/10.1029/2008GL035066>
- DeMets, C., Calais, E., & Merkouriev, S. (2017). Reconciling geodetic and geological estimates of recent plate motion across the Southwest Indian Ridge. *Geophysical Journal International*, *208*, 118–133. <https://doi.org/10.1093/gji/ggw386>
- DeMets, C., Gordon, R., & Royer, J.-Y. (2005). Motion between the Indian, Capricorn and Somalian plates since 20 Ma: Implications for the timing and magnitude of distributed lithospheric deformation in the equatorial Indian Ocean. *Geophysical Journal International*, *161*(2), 445–468. <https://doi.org/10.1111/j.1365-246X.2005.02598.x>
- DeMets, C., Gordon, R. G., & Argus, D. F. (2010). Geologically current plate motions. *Geophysical Journal International*, *181*(1), 1–80. <https://doi.org/10.1111/j.1365-246X.2009.04491.x>
- DeMets, C., & Merkouriev, S. (2016). High-resolution estimates of Nubia-Somalia plate motion since 20 Ma from reconstructions of the Southwest Indian Ridge, Red Sea and Gulf of Aden. *Geophysical Journal International*, *207*, 317–322. <https://doi.org/10.1093/gji/ggw276>
- DeMets, C., Merkouriev, S., & Sauter, D. (2015). High-resolution estimates of Southwest Indian Ridge plate motions, 20 Ma to present. *Geophysical Journal International*, *203*(3), 1495–1527. <https://doi.org/10.1093/gji/ggv366>
- Edwards, R. A., Minshull, T. A., & White, R. S. (2000). Extension across the Indian-Arabian plate boundary: The Murray Ridge. *Geophysical Journal International*, *142*(2), 461–477. <https://doi.org/10.1046/j.1365-246x.2000.00163.x>
- Ellouz Zimmermann, N., Lallemand, S., Castilla, R., Mouchot, N., Leturmy, P., Battani, A., et al. (2007). Offshore frontal part of the Makran accretionary prism (Pakistan) the Chamak Survey. In O. L. Lacombe, et al. (Eds.), *Thrust Belts and Foreland Basins: From Fold Kinematics to Hydrocarbon Systems* (pp. 349–364). Berlin: Springer. https://doi.org/10.1007/978-3-540-69426-7_18
- Embley, R. W., & Wilson, D. S. (1992). Morphology of the Blanco Transform Fault Zone-NE Pacific: Implications for its tectonic evolution. *Marine Geophysical Researches*, *14*(1), 25–45. <https://doi.org/10.1007/BF01674064>
- Exon, N. (2011). Detailed report on Indian Ocean IODP workshop, Goa, India, October 17–18, 2011. Retrieved from http://usssp-iodp.org/wp-content/uploads/Workshop_Report_India.pdf
- Fournier, M., Chamot-Rooke, N., Petit, C., Fabbri, O., Huchon, P., Maillot, B., & Lepvrier, C. (2008). In-situ evidence for dextral active motion at the Arabia-India plate boundary. *Nature Geoscience*, *1*(1), 54–58. <https://doi.org/10.1038/ngeo.2007.24>
- Fournier, M., Chamot-Rooke, N., Petit, C., Huchon, P., Al-Kathiri, A., Audin, L., et al. (2010). Arabia-Somalia plate kinematics, evolution of the Aden-Owen-Carlsberg triple junction, and opening of the Gulf of Aden. *Journal of Geophysical Research*, *115*, B04102. <https://doi.org/10.1029/2008JB006257>
- Fournier, M., Chamot-Rooke, N., Rodriguez, M., Huchon, P., Petit, C., Beslier, M.-O., & Zaragosi, S. (2011). Owen Fracture Zone: The Arabia-India plate boundary unveiled. *Earth and Planetary Science Letters*, *302*(1-2), 247–252. <https://doi.org/10.1016/j.epsl.2010.12.027>
- Fournier, M., Patriat, P., & Leroy, S. (2001). Reappraisal of the Arabia-India-Somalia triple junction kinematics. *Earth and Planetary Science Letters*, *189*(3-4), 103–114. [https://doi.org/10.1016/S0012-821X\(01\)00371-5](https://doi.org/10.1016/S0012-821X(01)00371-5)
- Fournier, M., Petit, C., Chamot-Rooke, N., Fabbri, O., Huchon, P., Maillot, B., & Lepvrier, C. (2008). Do ridge-ridge-fault triple junctions exist on Earth? Evidence from the Aden-Owen-Carlsberg junction in the NW Indian Ocean. *Basic Research*, *20*(4), 575–590. <https://doi.org/10.1111/j.1365-2117.2008.00356.x>
- Gaedicke, C., Prexl, A., Schlüter, H. U., Roeser, H., & Clift, P. (2002). Seismic stratigraphy and correlation of major regional unconformities in the northern Arabia Sea. In P. D. Clift, D. Kroon, C. Gaedicke, & J. Craig (Eds.), *The tectonic and climatic evolution of the Arabian Sea region Geological Society Special Publication* (Vol. 195, pp. 25–36). <https://doi.org/10.1144/GSL.SP.2002.195.01.03>
- Gaina, C., van Hinsbergen, D. J. J., & Spakman, W. (2015). Tectonic interactions between India and Arabia since the Jurassic reconstructed from marine geophysics, ophiolite geology, and seismic tomography. *Tectonics*, *34*, 875–906. <https://doi.org/10.1002/2014TC003780>
- Gordon, R. G., & DeMets, C. (1989). Present-day motion along the Owen fracture zone and Dalrymple trough in the Arabian Sea. *Journal of Geophysical Research*, *94*, 5560–5570. <https://doi.org/10.1029/JB094iB05p05560>
- Hayman, N., Grindlay, N., Perfit, M., Mann, P., Leroy, S., & Mercier de Lépinay, B. (2011). Oceanic core complex development at the ultraslow spreading Mid-Cayman Spreading Centre. *Geochemistry, Geophysics, Geosystems*, *12*, Q0AG02. <https://doi.org/10.1029/2010GC003240>
- Henstock, T. J., & Minshull, T. A. (2004). Localized rifting at Chagos bank in the India-Capricorn plate boundary zone. *Geology*, *32*(3), 237–240. <https://doi.org/10.1130/G19850.1>
- Iaffaldano, G., Bunge, H.-P., & Dixon, T. H. (2006). Feedback between mountain belt growth and plate convergence. *Geology*, *34*(10), 893–896. <https://doi.org/10.1130/G22661.1>
- Iaffaldano, G., & DeMets, C. (2016). Late Neogene changes in North America and Antarctica absolute plate motions inferred from the Mid-Atlantic and Southwest Indian Ridges spreading histories. *Geophysical Research Letters*, *43*, 8466–8472. <https://doi.org/10.1002/2016GL070276>

- Iaffaldano, G., Husson, L., & Bunge, H.-P. (2011). Monsoon speeds up Indian plate motion. *Earth and Planetary Science Letters*, 304(3-4), 503–510. <https://doi.org/10.1016/j.epsl.2011.02.026>
- Krishna, K. S., Bull, J. M., & Scrutton, R. A. (2009). Early (pre-8Ma) fault activity and temporal strain accumulation in the central Indian Ocean. *Geology*, 37(3), 227–230. <https://doi.org/10.1130/G25265A.1>
- Lambotte, S., Lyon-Caen, H., Bernard, P., Deschamps, A., Patau, G., Necessian, A., et al. (2014). Reassessment of the rifting process in the Western Corinth Rift from relocated seismicity. *Geophysical Journal International*, 194, 1822–1844. <https://doi.org/10.1093/gji/ggu096>
- Leroy, S., Razin, P., Autin, J., Bache, F., d'Acremont, E., Watremez, L., et al. (2010). From rifting to oceanic spreading in the Gulf of Aden: A synthesis. *Arabian Journal of Geoscience*. <https://doi.org/10.1007/s12517-011-0475-4>
- Ligi, M., Bonatti, E., Bortoluzzi, G., Carrara, G., Fabretti, P., Gilod, D., et al. (1999). Bouvet triple junction in the South Atlantic: Geology and evolution. *Journal of Geophysical Research*, 104, 29,365–29,385. <https://doi.org/10.1029/1999JB900192>
- Ligi, M., Bonatti, E., Bortoluzzi, G., Cipriani, A., Cocchi, L., Caratori Tontini, F., et al. (2012). Birth of an ocean in the Red Sea: Initial pangs. *Geochemistry, Geophysics, Geosystems*, 13, Q08009. <https://doi.org/10.1029/2012GC004155>
- Ligi, M., Bonatti, E., Bosthworth, W., Cai, Y., Cipriani, A., Palmiotta, C., et al. (2018). Birth of an ocean in the Red Sea: Oceanic-type basaltic melt intrusions precede continental rupture. *Gondwana Research*, 54, 150–160. <https://doi.org/10.1016/j.gr.2017.11.002>
- Ligi, M., Bonatti, E., Tontini, F. C., Cipriani, A., Cocchi, L., Schettino, A., et al. (2011). Initial burst of oceanic crust accretion in the Red Sea due to edge-driven mantle convection. *Geology*, 39(11), 1019–1022. <https://doi.org/10.1130/G32243.1>
- Maia, M., Sichel, S., Briais, A., Brunelli, D., Ligi, M., Ferreira, N., et al. (2016). Extreme mantle uplift and exhumation along a transpressive transform fault. *Nature Geoscience*, 9(8), 619–623. <https://doi.org/10.1038/NGEO2759>
- Mann, P. (2007). Global catalogue, classification and tectonic origins of restraining- and releasing bends on active and ancient strike-slip fault systems. *Geological Society of London, Special Publication*, 290(1), 13–142. <https://doi.org/10.1144/SP290.2>
- Mann, P., Hempton, M. R., Badley, D. C., & Burke, K. (1983). Development of pull-apart basins. *Journal of Geology*, 91(5), 529–554. <https://doi.org/10.1086/628803>
- Matthews, D. H. (1966). The Owen fracture zone and the northern end of the Carlsberg Ridge. *Philosophical Transactions of the Royal Society of London Series A*, 259(1099), 172–186. <https://doi.org/10.1098/rsta.1966.0005>
- McHugh, C. M. G., Seeber, L., Cormier, M.-H., Dutton, J., Gagatay, N., Polonia, A., et al. (2006). Submarine earthquake geology along the North Anatolia Fault in the Marmara Sea, Turkey: A model for transform basin sedimentation. *Earth and Planetary Science Letters*, 248(3-4), 661–684. <https://doi.org/10.1016/j.epsl.2006.05.038>
- McKenzie, D. P., Davies, D., & Molnar, P. (1970). Plate tectonics of the Red Sea and East Africa. *Nature*, 226(5242), 243–248. <https://doi.org/10.1038/226243a0>
- McKenzie, D. P., & Morgan, W. J. (1969). Evolution of triple junctions. *Nature*, 224(5215), 125–133. <https://doi.org/10.1038/224125a0>
- Merkouriev, S., & DeMets, C. (2006). Constraints on Indian plate motion since 20 Ma from dense Russian magnetic data: Implications for Indian plate dynamics. *Geochemistry, Geophysics, Geosystems*, 7, Q02002. <https://doi.org/10.1029/2005GC001079>
- Miranda, J. M., Luis, J. F., Lourenço, N., & Goslin, J. (2010). Distributed deformation close to the Açores Triple 'Point'. *Marine Geology*, 355, 27–35.
- Molnar, P., & Stock, J. (2009). Slowing of India's convergence with Eurasia since 20 Ma and its implications for Tibetan mantle dynamics. *Tectonics*, 28, TC3001. <https://doi.org/10.1029/2008TC002271>
- Mountain, G. S., & Prell, W. L. (1990). A multiphase plate tectonic history of the southeast continental margin of Oman, The Geology and Tectonics of the Oman Region, edited by Robertson, A. H. F., Searle, M. P. and Ries, A. C. *Geological Society Special Publications*, 49, 725–743.
- Patriat, P., Sloan, H., & Sauter, D. (2008). From slow to ultraslow: A previously undetected event at the Southwest Indian Ridge at ca. 24 Ma. *Geology*, 36(3), 207–210. <https://doi.org/10.1130/G24270A.1>
- Pondard, N., & Barnes, P. M. (2010). Structure and paleoearthquake records of active submarine faults, Cook Strait, New Zealand: Implications for fault interactions, stress loading, and seismic hazard. *Journal of Geophysical Research*, 115, B12320. <https://doi.org/10.1029/2010JB007781>
- Rebesco, M., Hernández-Molina, F. J., Van Rooij, D., & Wahlin, A. (2014). Contourites and associated sediments controlled by deep-water circulation processes: State of the art and future considerations. *Marine Geology*, 352, 111–154.
- Rodriguez, M., Chamot-Rooke, N., Fournier, M., Huchon, P., & Delescluse, M. (2013). Mode of opening of an oceanic pull-apart: The 20°N Basin along the Owen Fracture Zone (NW Indian Ocean). *Tectonics*, 32, 1343–1357. <https://doi.org/10.1002/tect.20083>
- Rodriguez, M., Chamot-Rooke, N., Huchon, P., Fournier, M., & Delescluse, M. (2014). The Owen Ridge uplift in the Arabian Sea: Implications for the sedimentary record of Indian monsoon in Late Miocene. *Earth and Planetary Science Letters*, 394, 1–12. <https://doi.org/10.1016/j.epsl.2014.03.011>
- Rodriguez, M., Chamot-Rooke, N., Huchon, P., Fournier, M., Lallemand, S., Delescluse, M., et al. (2014). Tectonics of the Dalrymple Trough and uplift of the Murray Ridge (NW Indian Ocean). *Tectonophysics*, 636, 1–17. <https://doi.org/10.1016/j.tecto.2014.08.001>
- Rodriguez, M., Fournier, M., Chamot-Rooke, N., Huchon, P., Bourget, J., Sorbier, M., et al. (2011). Neotectonics of the Owen Fracture Zone (NW Indian Ocean): Structural evolution of an oceanic strike-slip plate boundary. *Geochemistry, Geophysics, Geosystems*, 12, Q12006. <https://doi.org/10.1029/2011GC003731>
- Rodriguez, M., Fournier, M., Chamot-Rooke, N., Huchon, P., Zaragosi, S., & Rabaute, A. (2012). Mass wasting processes along the Owen Ridge (Northwest Indian Ocean). *Marine Geology*, 326-328, 80–100. <https://doi.org/10.1016/j.margeo.2012.08.008>
- Rodriguez, M., Huchon, P., Chamot-Rooke, N., Fournier, M., & Delescluse, M. (2016). Tracking the Paleogene India-Arabia plate boundary. *Marine and Petroleum Geology*, 72, 336–358. <https://doi.org/10.1016/j.marpetgeo.2016.02.019>
- Shedd, W., Boswell, R., Frye, M., Godfriaux, P., & Kramer, K. (2012). Occurrence and nature of 'bottom simulating reflectors' in the northern Gulf of Mexico. *Marine and Petroleum Geology*, 34(1), 31–40. <https://doi.org/10.1016/j.marpetgeo.2011.08.005>
- Shipboard Scientific Party (1974). Site 222. In R. B. Whitmarsh, O. E. Weser, & D. A. Ross (Eds.), *DSDP Init. Repts*, leg 23 (pp. 211–289). <https://doi.org/10.2973/dsdp.proc.23.106>
- Shipboard Scientific Party (1989). Site 722. In W. L. Prell, et al. (Eds.), *Proc. ODP, Init. Repts* (pp. 255–317). College Station, TX: Ocean Drilling Program.
- Stein, C. A., & Cochran, J. (1985). The transition between the Sheba Ridge and the Owen Basin: Rifting of an old oceanic lithosphere. *Geophysical Journal of the Royal Astronomical Society*, 81(1), 47–74. <https://doi.org/10.1111/j.1365-246X.1985.tb01350.x>
- ten Brink, U. S., & Ben-Avraham, Z. (1989). The anatomy of a pull-apart basin: Seismic reflection observations of the Dead Sea Basin. 8(2), 333–350. <https://doi.org/10.1029/TC008i002p00333>
- ten Brink, U. S., & Flores, C. H. (2012). Geometry and subsidence history of the Dead Sea basin: A case for fluid induced mid-crustal shear zone? *Journal of Geophysical Research*, 117, B01406. <https://doi.org/10.1029/2011JB008711>

- Weissel, J. K., Anderson, R. N., & Geller, C. A. (1980). Deformation of the Indo-Australian plate. *Nature*, *287*(5780), 284–291. <https://doi.org/10.1038/287284a0>
- Weissel, J. K., Childers, V. A., & Karner, G. D. (1992). Extensional and compressional deformation of the lithosphere in the light of ODP drilling in the Indian Ocean. In R. A. Duncan, et al. (Eds.), *Synthesis of Results from Scientific Drilling in the Indian Ocean, Geophysical Monograph*, (Vol. 70, pp. 127–156). Washington, DC: American Geophysical Union.
- Wiens, D. A., Demets, C., Gordon, R. G., Stein, S., Argus, D., Engeln, J. F., et al. (1985). A diffuse plate boundary model for Indian ocean tectonics. *Geophysical Research Letters*, *12*, 429–432. <https://doi.org/10.1029/GL012i007p00429>
- Wilson, T. J. (1965). A new class of faults and their bearing on continental drift. *Nature*, *207*(4995), 343–347. <https://doi.org/10.1038/207343a0>